A Study on Vibration Isolation in a Wind Turbine Subjected to Wind and Seismic Loading

by

Chad Van der Woude

A thesis

presented to the University of Waterloo

in fulfillment of the

thesis requirement for the degree of

Master of Applied Science

in

Civil Engineering

Waterloo, Ontario, Canada, 2011

Declaration

I hereby declare that I am the sole author of this thesis. This is a true copy of this thesis, including any required final revisions, as accepted by my examiners.

I understand that this thesis may be made electronically available to the public.

Abstract

The primary loading on wind turbines is in the lateral direction and is of a stochastic nature, due to wind and seismic forces. As turbines grow larger, they experience proportionally larger lateral forces. Large forces require larger section sizes and overall weight of the turbine. The objective of this study is to investigate the use of vibration isolation as a structural control measure to minimize the overall wind and seismic forces transmitted to the turbine. Passive control systems such as tuned mass dampers have previously been proposed to mitigate response to wind loading but have not generally been evaluated under seismic loading.

This thesis discusses the potential use of a non-linear vibration isolator just below the wind turbine nacelle to decrease the structural response of the turbine under wind and seismic loading. The structural idealization of the wind turbine structure and the applied loading are presented. The force-displacement properties of the vibration isolator are discussed and the equations of motion are modified to include the isolator.

A finite element model is created which includes wind and seismic loading and incorporates a vibration isolator. Simulations are performed to determine a number of key structural response variables without the vibration isolator, and with a vibration isolator having varied force-displacement properties. The changes in those key response variables are presented and discussed. It is concluded that vibration isolation is a viable method for reducing structural response of wind turbines. Some practical concerns and areas of future research are discussed.

Acknowledgements

TABLE OF CONTENTS

LIST OF FIGURES

LIST OF TABLES

1. Introduction

The increasing size, power generation demands, and ubiquity of wind turbines has lead naturally to increasing concerns regarding their structural integrity. Maintaining and growing the wind energy industry in Canada and worldwide requires careful application of structural engineering principles to the design of wind turbines. Given the current demand for energy, it is inevitable that large wind turbines will eventually be adopted in seismically active regions, including the west coast of British Columbia in Canada.

In addition to carrying their own weight, wind turbine structures must withstand lateral loads due to wind and seismic events. Seismic loading is not design-driving for wind turbines in most parts of the world, a fact that is reflected in design standards such as IEC 61400-1. However, seismic loading and response of turbine structures has become a greater concern as wind farms have been proposed in seismically active areas, including parts of India and the west coast of North America. It is expected that turbines installed in such seismically active areas would require substantial strengthening of the towers, blades and foundations to withstand the combined effects of wind and seismic forces. Instead, the proposed study investigates the use of vibration isolation in reducing the overall wind and seismic forces experienced by large turbines, as an economical alternative to traditional strengthening methods.

A typical wind turbine structure is shown in Figure 1, with its components labelled.
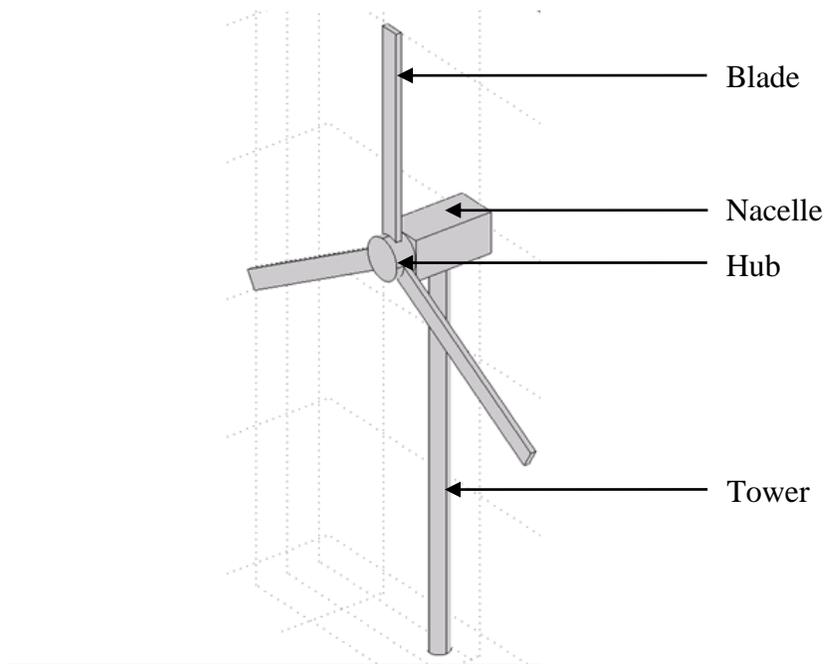
Figure 1. Schematic isometric view of typical wind turbine.

The aerodynamic properties of the blades convert the oncoming wind into along-wind forces and tangential forces, which cause rotation of the blades and hub. The hub connects the blades to a shaft, which turns a generator within the nacelle, to convert the rotational energy into usable electrical energy. The tower supports the nacelle at a height where the wind speed will produce the desired power.

Areas of structural concern for wind turbines include overall integrity of the blades and tower, fatigue life of the blades and tower, displacement of the structure as a whole, and acceleration of the nacelle. Researchers have previously investigated the probabilities of extreme loading and reliability of wind turbines (e.g. Dueñas-Osorio, 2008), and proposed the use of tuned mass dampers and tuned liquid column dampers, among others, to mitigate dynamic response (e.g.

Murtagh, 2008; Colwell, 2009). However, the effectiveness of structural control measures specific to seismic loading has not been well-studied.

This thesis proposes the use of lateral vibration isolation as a measure to reduce turbine response to seismic and wind loading. The key idea of vibration isolation is to introduce a flexible element within the structure-foundation system to lengthen the natural period and filter the frequencies propagating between the isolated and un-isolated parts of the structure. Usually, in buildings, a vibration isolator is placed between the base of the building and the ground to protect against seismic loading, as shown in Figure 2.

Isolated Structure at Rest   Isolated Structure under Loading
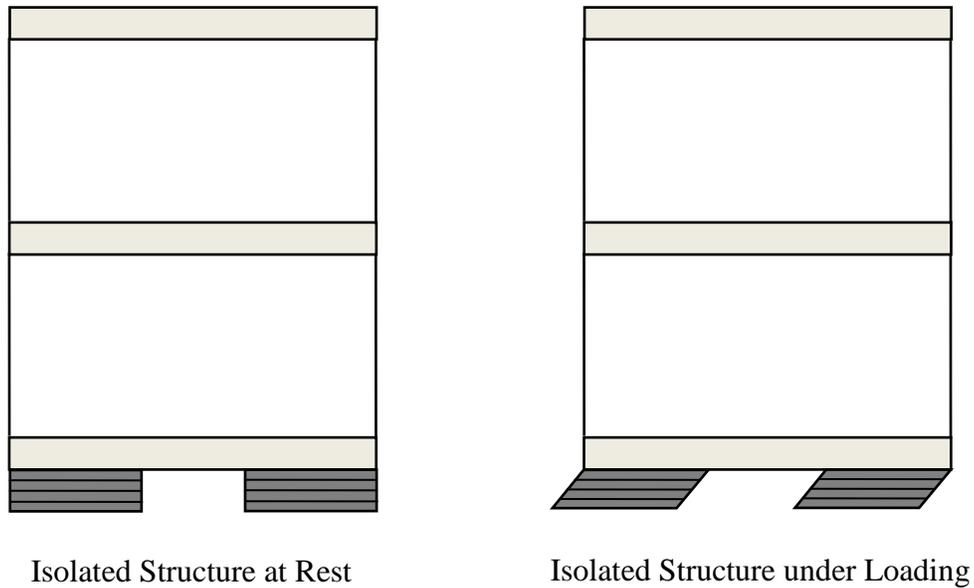
Figure 2. Schematic of base isolation in a building structure.

By isolating the structure from the ground, the fundamental lateral period of the structure is lengthened, typically to between 2.5 and 4 seconds, thereby reducing the seismic energy

transmitted to the structure. Due to the flexibility, a base-isolated system undergoes significant displacement across the isolator, with relatively little structural deformation as compared to the un-isolated system (Naiem, 1999). In the proposed design, the location of the isolator is shown schematically in Figure 3.
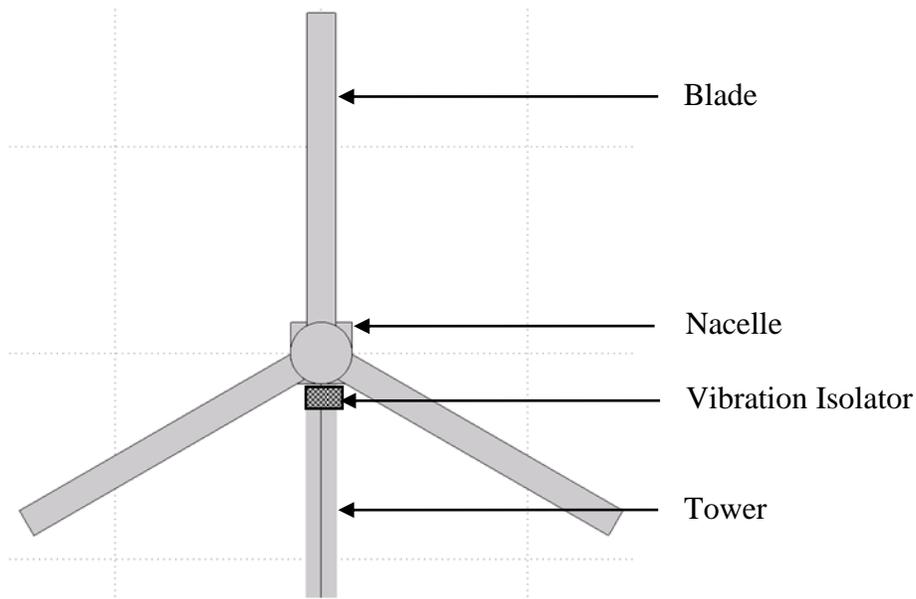
Figure 3. Front view schematic of typical wind turbine showing isolator location.

The vibration isolator allows for differential lateral motion between the top of the tower and the bottom of the nacelle and lengthens the effective period of the blade-nacelle system. This design could potentially lead to decreases in acceleration of the nacelle and base shear and moment in the blades, among other key response parameters, particularly when the turbine is subjected to seismic loading. Base isolation systems for buildings are typically intended to undergo large displacements under seismic loading but not under wind loading. The use of a vibration isolator

for a wind turbine structure is complicated by the relative magnitude of wind loading relative to seismic loading.

Vibration isolators may variously include elements having elastic behaviour, as in springs or rubber pads; viscous behaviour, as in fluid dampers; elasto-plastic behaviour, as in steel yielding assemblies; or other force-displacement characteristics. Viscous and elasto-plastic elements introduce damping and supplement the performance of the system compared to linear isolators. This thesis investigates the case of a vibration isolator having a linear elastic element, a viscous element, and an elasto-plastic element in parallel. In a real isolator, this idealization might apply to a device which has a linear elastic component due to low-damping rubber bearing pads, viscous damping due to a supplemental liquid piston damper, and an elasto-plastic force due to a supplemental lead plug which yields at some level of displacement. The properties of the isolator are varied in this investigation, and the effects on the key response parameters of the turbine structure are investigated using COMSOL Multiphysics, a commercial finite element suite.

1.1 Objective and Scope

The objective of this thesis is to present a numerical study that demonstrates quantitatively the effectiveness of using vibration isolation to modify the structural response of a specific wind turbine subjected to wind and seismic loading in the along-wind direction. It is the intent of the author to show that a vibration isolator, properly designed and implemented, could be valuable in decreasing structural response in wind turbines. The decrease in response would allow for optimization of wind turbine structural proportions, fatigue life, and availability, particularly in seismically active regions. Vibration isolation could be used to make construction of wind

turbines in seismically active areas more feasible and economical. The isolator could be considered in the initial design of the turbine to allow for more efficient use of material or a longer fatigue life. Vibration isolators could also be retrofitted to existing wind turbine designs to realize increases in load-carrying capacity or fatigue life.

The scope of this thesis is to present the results of the aforementioned study. The properties of this turbine are chosen to be similar to contemporary turbine structures, but are not representative of a specific industrial turbine design. As such, the numeric values of the responses are considered secondary to the relative increases and decreases in response. Seismic and wind loads are applied to the structure in the along-wind direction only. Implementation of vibration isolation in a full-scale industrial-class wind turbine would require significant study, computational effort, testing and monitoring. This thesis is intended to stimulate designers to consider this possibility using qualitative examination of quantitative data.

2. Background

Rotating structures that extract power from the wind have been in use for over 3000 years in the form of windmills (Burton, 2001). Windmills have been used for many centuries for tasks such as grinding and pumping, and are now also commonly used for generation of electricity. Many configurations have been conceptualized, designed and used for power generation, including those which rotate about vertical or horizontal axes and with varying numbers and types of blades. This thesis will focus on three-bladed horizontal-axis wind turbines, which are commonly used for industrial power generation.

2.1 Wind Turbine Structures

The wind turbines considered in this thesis consist of three blades connected at a rigid hub which is attached to a nacelle containing equipment used to generate electricity. The nacelle is supported by a tubular steel tower. An isometric view of a typical turbine with its components labelled was previously shown in Figure 1.

The turbine tower is cantilevered from the ground while the blades are cantilevered from the hub. The structure can be idealized as fully coupled, in which the structural response of the blades and tower are studied simultaneously; or uncoupled, in which the structural response of the blade is calculated assuming it is a fixed-base cantilever and the structural response of the tower is calculated assuming it is a fixed-base cantilever carrying a point mass and inertia at its tip.

When the turbine is parked, it can be analysed as a structure with fixed geometry, but when the turbine is operational the analysis is complicated by the time-dependent geometry of the

structure. In the operational case, the natural frequencies and vibration modes of the blades and tower can be formulated separately. The blade and tower vibration modes, then, will not be orthogonal to one another, and modal coupling must be accounted for (Burton, 2001). When the turbine is operating, the rotation of the blades causes a centrifugal stiffening effect which increases the effective stiffness, and thus the natural frequencies, of the blades (Burton, 1999). Accurate modelling of the turbine structure is of key importance to effective design and analysis.

2.2 Wind Turbine Loading

In this study, the primary lateral loads on a wind turbine are caused by wind and seismic events. These loads are of a stochastic nature and must be treated using probabilistic methods. Guidelines on analysis and load calculations are available in many references and design standards. References include the Wind Energy Handbook (Burton, 2001) and Aerodynamics of Wind Turbines (Hansen, 2008). Design standards for wind turbines include the International Electrotechnical Commission's IEC 61400-1 *Wind turbines – Part 1: Design Guidelines*, Germanischer Lloyd's *Regulation for the Certification of Wind Energy Conversion Systems*, and Danish Standard DS 472. This thesis will focus on IEC 61400-1.

Calculation of loads on wind turbine blades must be carried out taking into account the aerodynamics of the blade sections. This is accomplished using the Blade Element Momentum (BEM) theory which relates the oncoming wind speed and rotational speed of the blades to the along-wind and tangential forces applied to the blades (Hansen, 2008). Turbine blade sections for utility-class turbines are usually proprietary in nature, but some literature is available that discusses general trends in their parameters (Timmer, 2010).

IEC 61400-1 presents 22 design load cases associated with wind. The load cases are separated into 8 design situations: power production; power production plus occurrence of fault; start up; normal shutdown; emergency shutdown; parked (standing still or idling); parked and fault conditions; and transport, assembly, maintenance and repair. In each of these design situations, a number of wind conditions must be considered. The wind conditions specified include normal and extreme turbulent wind with specified wind speed and standard deviation, as well as a number of deterministic transient wind conditions including an extreme operating gust, extreme wind direction change, and extreme wind shear across the rotor.

For the turbulent wind cases, two wind simulation models are allowed by IEC 61400-1; the Mann uniform shear turbulence model and the Kaimal spectrum and exponential coherence model. The Mann model is significantly more complex and includes cross-correlation between wind speeds in all three spatial dimensions. In the Kaimal model, wind in each spatial direction is considered separately.

IEC 61400 does not provide minimum seismic requirements for standard turbines, as seismic loads are not expected to be design-driving in most parts of the world. Section 11.6 states that in cases where seismic loading is not excluded by local building codes, it may be addressed using the ground acceleration and response spectra of those local codes. The ground acceleration used for evaluation should be based on a 475-year recurrence period. The earthquake loading must be superposed with operational loading equal to the greater of loads during normal power production, averaged over the lifetime, and loads during emergency shutdown for a wind speed where the loads prior to shutdown are equal to those during normal power production. The number of vibration modes used for assessment must be in accordance with a recognized seismic

code, and in the absence of such a code, consecutive modes with a total modal mass of 85% of the total mass shall be used.

Annex C of IEC 61400-1 presents a simplified method which may be used if the seismic action causes significant loading only on the tower. In this case, the normalized local design response spectrum should be used to determine the acceleration at the first tower bending eigen-frequency assuming 1% critical damping. This acceleration is used to calculate the load on a system in which the total rotor, nacelle and 50% of the tower mass is concentrated at the tower head. The resulting loads are added to the characteristic loads calculated for an emergency stop at rated wind speed. If the turbine can withstand this combined loading, no further analysis is needed; otherwise, a more detailed investigation should be carried out. This method is a significant simplification which assumes that the tower response is confined to the fundamental mode. The use of a conservatively large head mass including 50% of the tower mass is used in IEC 61400-1 to justify the simplification. IEC 61400-1 does not provide guidance on isolation system design for turbines, as these technologies are not yet common-place and have not been studied in literature. Hence, a detailed non-linear time-history analysis approach is pursued in this thesis.

2.3 Vibration Isolation

Vibration isolation, as previously discussed, is commonly used for base isolation of buildings against seismic loading. Some commonly used isolator types include low-damping rubber bearings (LDRB), lead-rubber bearings (LRB), and friction pendulum systems (FPS). Section views of these three isolator types are shown in Figure 4.

(a)

(b)

Top Plate

Rubber

Steel Sheet

Bottom Plate

Lead Core

(c)

Articulated Slider

Concave Stainless
Steel Sliding Surface
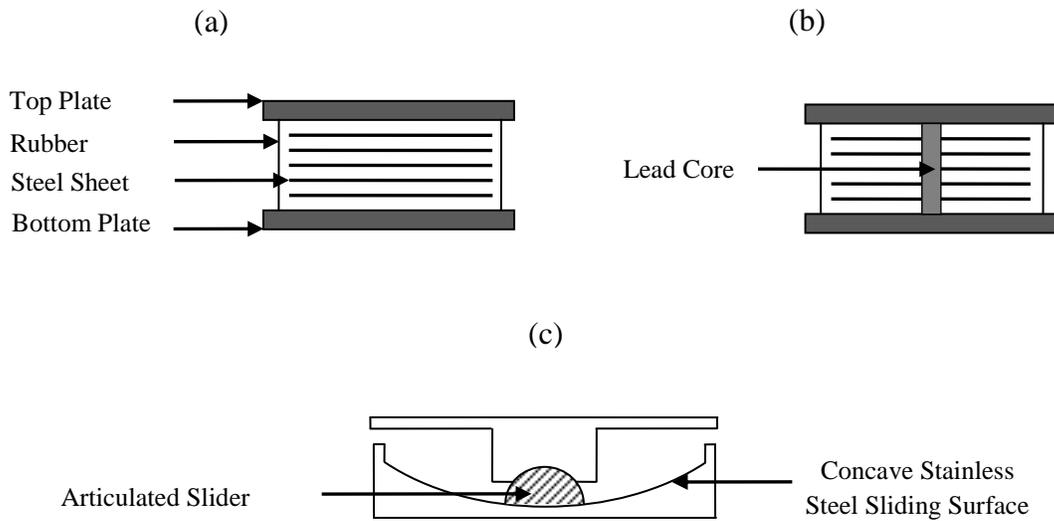
Figure 4. Section views of various types of vibration isolator.

Low-damping rubber bearings, shown in Figure 4(a), are comprised of alternating layers of natural or synthetic rubber and thin steel sheets. LDRBs are flexible in the lateral direction to provide seismic protection, while the steel sheets constrain the rubber layers to give a higher vertical stiffness. The rubber used has very little inherent damping, so the force-displacement behaviour of the isolator is almost exactly linear (Naiem, 1999). Lead-rubber bearings are similar to LDRBs, with the addition of one or multiple lead cores as shown in Figure 4(b). The yielding of the lead allows for energy dissipation under large displacements. The lateral force-displacement behaviour of LRBs is typically modelled using a bilinear stiffness model, where the initial stiffness is due to the combined resistance of the bearing and the lead, while the post-yield stiffness is due to the resistance of the rubber after the lead has yielded (Naiem, 1999). Friction pendulum systems use an articulated slider which translates on a spherical surface, as shown in Figure 4(c). As the isolator displaces laterally, it is forced upward and the geometry of the

11

isolator causes a restoring force. The force-displacement behaviour of an FPS is typically modelled using a bilinear stiffness model (Naiem, 1999).

The Bouc-Wen model of hysteresis (Wen, 1976) is a mathematical model used to quantify the force-displacement relationship of a system in which the current state of the system is based on its previous states. A non-linear first order differential equation must be solved to determine the isolator force at any given time. The parameters of the model, properly selected, are capable of emulating bilinear stiffness behaviour (Marano, 2007). For this thesis, the Bouc-Wen model is used to model the behaviour of the vibration isolator.

2.4 Literature Review

Much literature has been devoted to the analysis of wind turbine structures under wind loading, including scholarly articles; design guidelines like IEC 61400; and books such as the Wind Energy Handbook (Burton, 2001) and Aerodynamics of Wind Turbines (Hansen, 2008). Studies have been carried out to perform and evaluate designs, study the effects of coupling between the blades and the tower (Murtagh, 2005), evaluate key parameters of structural response (Murtagh, 2005; Dueñas-Osorio, 2008), and propose and evaluate the use of control devices to decrease those parameters, including tuned mass dampers and liquid column dampers (Murtagh, 2008; Colwell, 2009). Some studies have been performed which focus on seismic loading and response (Witcher, 2005; Prowell, 2008), but mitigation of seismic effects using supplementary damping or control devices has not been reported.

Many books have been published which deal in whole or part with the structural analysis and design of wind turbines. In particular, the Wind Energy Handbook (Burton, 2001) provides

12

detailed information on many aspects of wind energy, including aerodynamics, structural analysis and design of turbine towers and blades, turbine performance, wind farm layout and electrical systems. Aerodynamics of Wind Turbines (Hansen, 2008) discusses aspects including aerodynamics, structural analysis and design, simulation of wind loads, and fatigue analysis.

Simulation of turbulent wind involves the use of power spectral density (PSD) functions to determine the frequency content of the wind speed time-history, and coherence functions to quantify the correlation between wind speed time-histories at spatially separated points (Hansen, 2008). It is possible to develop a rotationally sampled PSD function corresponding to the wind speed fluctuations that would be seen by a rotating turbine blade (Burton, 2001). It is also possible to emulate this effect by simulating wind speed time-histories at a number of points in a radial grid originating at the centre of the hub and successively changing which time-history is being applied to the blade as it rotates. The latter method requires more computation, as it generates wind speed time-histories which are not being applied to the blades at all times. The method can be made more efficient by only computing the numeric values of wind speed at the times they are needed for each point (Veers, 1988).

For the simplified uncoupled case where the mass of the blades, hub and nacelle are considered to be lumped at the top of the tower, it has been shown that analytical solution for the natural frequencies and mode shapes of the tower is possible, although the continuous mode shapes derived are not orthogonal (Murtagh, 2004). For the first few vibration modes, the analytical solution may be useful to avoid the computational effort of creating a finite element model. However, investigations have also found that for wind turbines subjected to wind loading in the along-wind direction, solutions which do not take into account blade-tower coupling may provide unconservative results (Murtagh, 2005). Blade-tower coupling can increase the structural

13

response in the tower in some cases. This effect is mitigated somewhat by the stiffening effect caused by the rotation of the blades (Naguleswaran, 1994). The investigations by Murtagh utilized a substructure approach in which the dynamic properties of the blades and the tower were formulated separately, then the sub-structures were coupled using constraint equations and analyzed together. This approach has been used in various forms and is particularly useful for structures with many degrees of freedom (Hurty, 1965; Craig, 2006).

In addition to the structural integrity of turbines under extreme wind loading, it has been shown that unavailability of wind turbines due to excessive acceleration at hub-height may be a significant concern, as critical acceleration levels for certain components may be exceeded at wind speeds below the shutdown threshold (Dueñas-Osorio, 2008). Passive control of turbines using a tuned mass damper (TMD) has been proposed and shown to be effective in decreasing structural response in a numerical model which incorporated blade-tower coupling (Murtagh, 2008). It has also been shown that for offshore wind turbines under wind and wave excitations, the use of a tuned liquid column damper (TLCD) could reduce structural response by over 50% and dramatically improve the fatigue life of the steel tower structure (Colwell, 2009).

With regard to seismic loading of wind turbines, literature is scarce. Although in most cases wind loading is more critical than seismic loading, new technologies like advanced control systems for turbine blades are being used to decrease the amount of structural wind loading which must be carried relative to the amount of power produced. As the wind loading of the structure is decreased through the judicious use of technology, seismic loading may become relatively more important for structural analysis and design, even in areas of moderate seismicity (Prowell, 2009). Some research is currently underway to quantify wind turbine structural response to seismic loading, through theoretical work and empirical testing using full-scale shake

table testing for smaller turbines (Prowell, 2008). Simulation of structural response to seismic events may be carried out by the generation of artificial time histories of ground acceleration which are fitted to match a design response spectrum, a method which is implemented in the GH Bladed wind turbine simulation package (Witcher, 2005). It is of note that individual synthetic ground motion time histories are not generally representative of actual individual seismic events, as they are scaled to fit an idealized response spectrum and the associated ground displacement may be unrealistic. Thus, when using synthetic time histories, it is important to perform many simulations and examine the ensemble statistical properties (Naiem, 1999).

As previously discussed, a common method of decreasing seismic response of building structures is the use of base isolation, in which isolation devices are used to create a flexible layer at the base of the structure, changing the fundamental mode of vibration from one dominated by deformation of the structure to one dominated by a large displacement across the isolation layer with relatively little structural deformation (Naiem, 1999). The isolation elongates the natural period of the structure, thereby attracting lower seismic forces compared to its un-isolated counterpart. The Bouc-Wen model is commonly used to mathematically model vibration isolators and other hysteretic systems, in which the state of the system at a given time is dependent on its state at a previous time. This model, introduced by Bouc in 1971 and extended by Wen in 1976, provides a non-linear relationship between the force applied to the isolator and the displacement of the isolator. This relationship is defined by introducing a variable known as the hysteretic displacement, whose value is the solution to a first-order non-linear differential equation (Ismail, 2009). The Bouc-Wen model allows for mathematically simple representation of many types of force-displacement behaviour, including bilinear stiffness, with model parameters corresponding to yield displacement and sharpness of the yield transition.

15

Simulations of base isolation in buildings and bridges using the Bouc-Wen model have been conducted extensively in the literature (e.g. Narasimhan, 2006; Marano, 2007).

The concept of partial mass isolation (PMI) was proposed as a method of decreasing the seismic response of a building structure (Ziyaeifar, 1998). Rather than providing isolation at the base, as is typical for low-rise structures, it was proposed that one storey of a mid-to-high-rise building work as an isolation storey with a lower stiffness than those around it, coupled with a viscous damping element. Changes in the natural frequencies and modes in the structure, with favourable effects on structural response, were demonstrated. That work demonstrated the effect of the isolation system on the natural modes and frequencies of mid-height shear-dominated and tall flexural buildings, as well as results of dynamic analyses under recorded seismic ground motions. For a 50-storey building, it was shown that, although significant reductions in structural response could be realized, under certain circumstances the amount of energy put into the structural system could actually be increased due to the flexibility of the structure both above and below the isolator, necessitating careful choice of isolation properties. With proper detailing and energy dissipation, the isolation storey can effectively decrease structural response (Ziyaeifar, 1998).

This thesis proposes to incorporate a variant of partial mass isolation by isolating the blade-hub-nacelle system of a wind turbine from the tower. This use of isolation has the potential to significantly decrease seismic demand on a wind turbine structure, and based on a survey of existing literature, will be a novel contribution to the study of wind turbine structures under wind and seismic loading.

3. Theoretical Formulation

To investigate the behaviour of a wind turbine structure with a vibration isolator, it is necessary to formulate the equations of motion for an idealization of the structure, the loading applied to the structure, and the mathematical model of the isolator.

3.1 Wind Turbine Structural Idealization

Wind turbine towers and blades are slender in section compared to their lengths, and can thus be represented by Euler-Bernoulli beams whose structural response is characterized by flexural deformation. A schematic side-view of a wind turbine showing a simple structural idealization is shown in Figure 5.
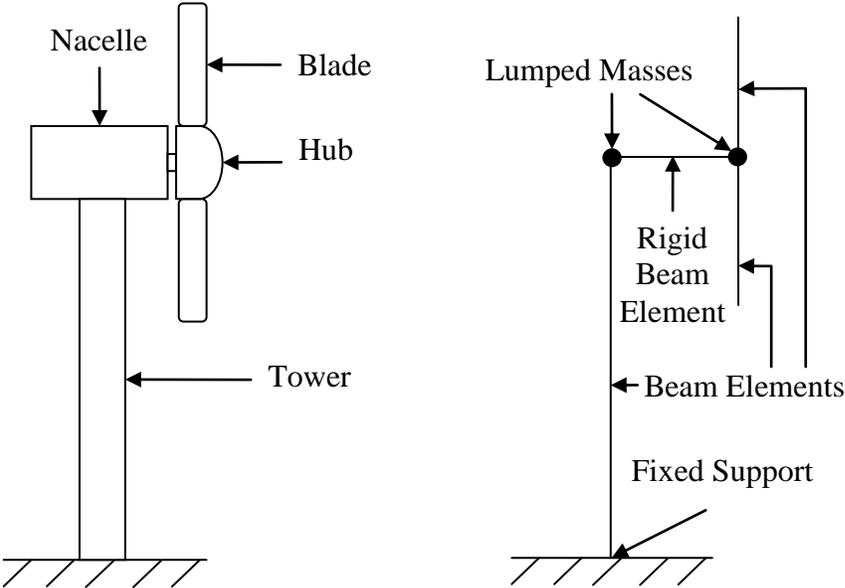
Figure 5. Typical wind turbine and structural idealization.

As shown, the wind turbine structure can be idealized using flexible beam elements for the tower and blades, a rigid element for the nacelle, and lumped masses to represent the nacelle and hub masses. The blade and tower elements have distributed stiffness and distributed mass. Assuming that the turbine is not operating, the behaviour of the beam elements is linear elastic, and damping is of a linear viscous type, the equations of motion of the structure can be written as

$$\mathbf{M\ddot{x} + C\dot{x} + Kx = F} \tag{1}$$

where $\mathbf{M}$ is the mass matrix of the structure,

                 $\mathbf{C}$ is the damping matrix of the structure,

                 $\mathbf{K}$ is the stiffness matrix of the structure,

                 $\mathbf{F}$ is the vector of applied forces,

                 $\mathbf{x}$ is the vector of nodal displacements of the structure, and

                 overdots   represent derivatives with respect to time.

The number of nodes and their location are determined by the discretization of the model domain. The equations of motion can be solved by modal analysis as a set of single degree of freedom systems or solved directly in the time domain using a numerical procedure such as Newmark's method (Craig, 2006).

When the blades are rotating, the problem is complicated by the fact that the system matrices $\mathbf{C}$ and $\mathbf{K}$ become time-dependent due to the periodic change in the geometry of the structure associated with blade rotation. Rotation of the blades can be implemented numerically by formulating the equations for the tower and rotor individually and defining a time-dependent

coupling between the base of the blades and the tip of the nacelle. The coordinate system used for this work is shown in Figure 6.
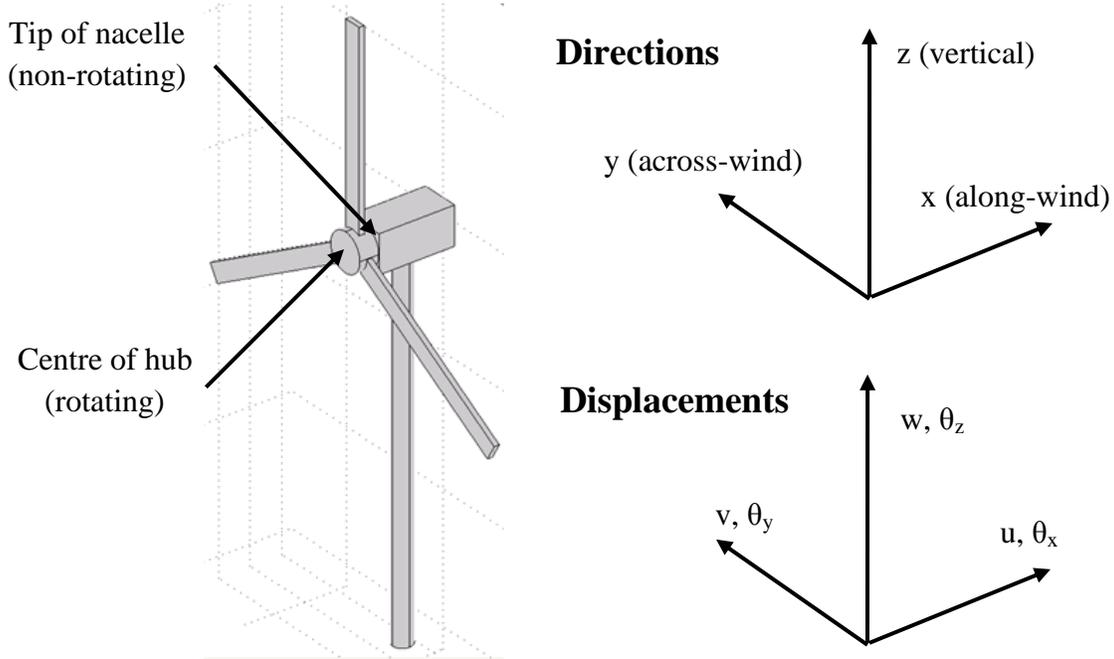
Figure 6. Coordinate system for wind turbine formulation.

Displacements are denoted by the letters u, v and w, while rotations are denoted by Greek letter theta, with subscript corresponding to the direction of the rotation axis with directional sense according to a right-hand screw rule. Denoting the displacements at the centre of the hub in rotating coordinates by the subscript r and the displacements at the tip of the nacelle in inertial coordinates by the subscript n, the constraints for rotation of the rotor can be written as

$$u_n = u_r \tag{2}$$

$$v_n = v_r \cos(\omega t) - w_r \sin(\omega t) \tag{3}$$

$$w_n = w_r \cos(\omega t) + y_r \sin(\omega t) \tag{4}$$

$$\theta_{x,n} = \theta_{x,r} \tag{5}$$

$$\theta_{y,n} = \theta_{y,r}\cos(\omega t) - \theta_{z,r}\sin(\omega t) \tag{6}$$

$$\theta_{z,n} = \theta_{z,r}\cos(\omega t) + \theta_{y,r}\sin(\omega t) \tag{7}$$

where ω is the rotational speed of the turbine, and

           t   is the time variable.

At time zero, the rotor is assumed to be oriented as in Figure 6, with one blade vertical. Rotation about the x-axis is constrained to be equal between the hub and the nacelle based on the assumption that the turbine is regulated to rotate at a fixed speed.

The rotation of the blades about the centre of the hub causes a tension force which varies along the length of the blade, given by (Naguleswaran, 1994)

$$F_t(r) = \int_r^{L+R_h} m(r)\omega^2 dr \tag{8}$$

where   r   is the distance from the centre of the hub to a point on the blade,

           L   is the length of the blade,

           R_h is the radius of the hub, and

           m(r)   is the mass per unit length at distance r from the centre of the hub.

The tensile force in the blades due to rotation increases the effective stiffness of the blades as well as their effective natural frequencies. Increasing the stiffness and natural frequencies of the blades changes their behaviour under seismic and wind loading, which have components at a broad range of frequencies. For loading having a significant frequency component near the natural frequency of the blades, the change in stiffness could have an appreciable effect on the structural response.

3.2 Wind Turbine Loading Idealization

The wind and seismic loading applied to a turbine structure are stochastic in nature. This section will discuss the theory behind wind and seismic loading and how they are applied to a turbine structure.

3.2.1 Wind Loading

In the simplest case, the applied wind force on a body is

$$F = \frac{1}{2} C_d \rho U^2 A \qquad (9)$$

where C_d is the drag coefficient of the body,

         ρ is the mass density of air,

         U   is the applied wind speed, and

         A   is the frontal area of the body.

Drag coefficients of many common shapes have been studied and tabulated in texts (e.g. Simiu, 1996). Since the wind speed varies with time, so does the applied force. To account for the variation in wind speed with height above the ground, a power-law profile is commonly used. The Normal Wind Profile model in IEC 61400-1, for example, states that

$$V(z) = V_{hub}(z/z_{hub})^{\alpha} \tag{10}$$

where $V(z)$ is the wind speed at height z,

V_{hub} is the wind speed at hub height,

z is the height at which wind speed is calculated,

z_{hub} is the height of the centre of the hub, and

α is a power-law exponent, taken equal to 0.2.

Wind speed time-histories display rapid short-term variations, known as turbulence. As noted previously, the frequency content of this turbulence is usually characterized by a PSD function. The PSD function determines the magnitude of the component of the fluctuating wind speed at a given frequency. The Kaimal spectrum, as specified in IEC 61400-1, is

$$\frac{fS_k(f)}{\sigma_k^2} = \frac{4fL_k/V_{hub}}{(1 + 6fL_k/V_{hub})^{5/3}} \tag{11}$$

where S_k is the power spectral density corresponding to wind speeds in direction k,

f is the turbulence frequency in Hz,

σ_k is the standard deviation corresponding to direction k,

L_k is a length scale corresponding to direction k, and

22

V_{hub} is the wind speed at hub height.

For the along-wind or longitudinal direction, the standard deviation depends on the wind conditions under consideration. The Normal Turbulence model from IEC 61400-1, which is used in this study, specifies that

$$\sigma = I_{ref}(0.75V_{hub} + b) \tag{12}$$

where I_{ref} is a reference turbulence intensity, usually between 0.12 to 0.16 for standard wind turbine classes, and

     b   is a constant taken equal to 5.6 m/s.

IEC 61400-1 defines the length scale L_k at hub height z, for wind in the longitudinal direction, as

$$L_k = 8.1\Lambda_1 \tag{13}$$

where

$$\Lambda_1 = 0.7z \ \text{ for } \ z \le 60m \tag{14}$$

$$\Lambda_1 = 42m \ \text{ for } \ z \ge 60m \tag{15}$$

The correlation between two wind-speed time histories at spatially separated points is quantified using a coherence function, defined in IEC 61400-1 as

$$Coh(r, f) = \exp[-12((fr/V_{hub})^2 + (0.12r/L_c)^2)^{0.5}] \tag{16}$$

where   r   is the spatial distance between the two points, and

               L_c is the coherence scale parameter, equal to L_k for wind in the

               longitudinal direction.

Power spectral density and coherence can be used to generate a set of coherent time histories of wind speed at discrete points. The development of these time histories involves evaluating the magnitude of the frequency components of the wind speed and using randomly generated phase angles for each frequency. Time histories are generated as follows (Hansen, 2008).

First, a matrix **S** is created for each frequency such that

$$S_{jk} = Coh_{jk} \sqrt{S_{jj} S_{kk}} \tag{17}$$

where Coh_{jk} is the coherence between points j and k at the given

               frequency, and

               S_{jj} and S_{kk} are the respective power spectral densities at points j and k.

A lower triangular matrix **H** is created for each frequency by an iterative scheme such that

$$H_{11} = S_{11}^{1/2} \tag{18}$$

$$H_{21} = S_{21}/H_{11} \tag{19}$$

$$H_{22} = (S_{22} - H_{21}^2)^{1/2} \tag{20}$$

$$H_{31} = S_{31}/H_{21} \tag{21}$$

$$\vdots$$

$$H_{jk} = \left(S_{jk} - \sum_{l=1}^{k-1} H_{jl}H_{kl} \right) / H_{kk} \tag{22}$$

$$H_{kk} = \left(S_{kk} - \sum_{l=1}^{k-1} H_{kl}^2 \right)^{1/2} \tag{23}$$

The **H** matrix can be thought of as weighting factors for a set of unit Gaussian white noise inputs which will generate a set of output signals with the desired PSD and coherence (Veers, 1988). A complex vector $\mathbf{V} = \mathbf{V_j}(f_m)$ is then created where

$$\text{Re}\big(\mathbf{V_j}(f_m)\big) = \sum_{k=1}^{j} H_{jk}\cos\,(\varphi_{km}) \tag{24}$$

$$\text{Im}\big(\mathbf{V_j}(f_m)\big) = \sum_{k=1}^{j} H_{jk}\sin\,(\varphi_{km}) \tag{25}$$

which are transformed to

$$\text{Amp}_j(f_m) = \left(\text{Re}\big(\mathbf{V_j}(f_m)\big)^2 + \text{Im}\big(\mathbf{V_j}(f_m)\big)^2 \right)^{1/2} \tag{26}$$

$$\tan\big(\Phi_j(f_m)\big) = \frac{\text{Im}\big(\mathbf{V_j}(f_m)\big)}{\text{Re}\big(\mathbf{V_j}(f_m)\big)} \tag{27}$$

where   m   is an index corresponding to the frequency component under consideration, and

φ_{km} is a randomly generated phase angle between 0 and 2π corresponding to a given spatial point k and frequency m.

The wind time histories at the j points can then be computed as

$$U_j(t) = \overline{U} + \sum_{m=1}^{N/2} 2Amp_j(f_m)\cos(2\pi f_m t - \Phi_j(f_m)) \tag{28}$$

where   N/2   is the number of frequency components used in the simulation.

The corresponding blade loading is calculated using the lift and drag characteristics of the blade. The wind speeds seen by a rotating blade at a given cross-section are shown in Figure 7.
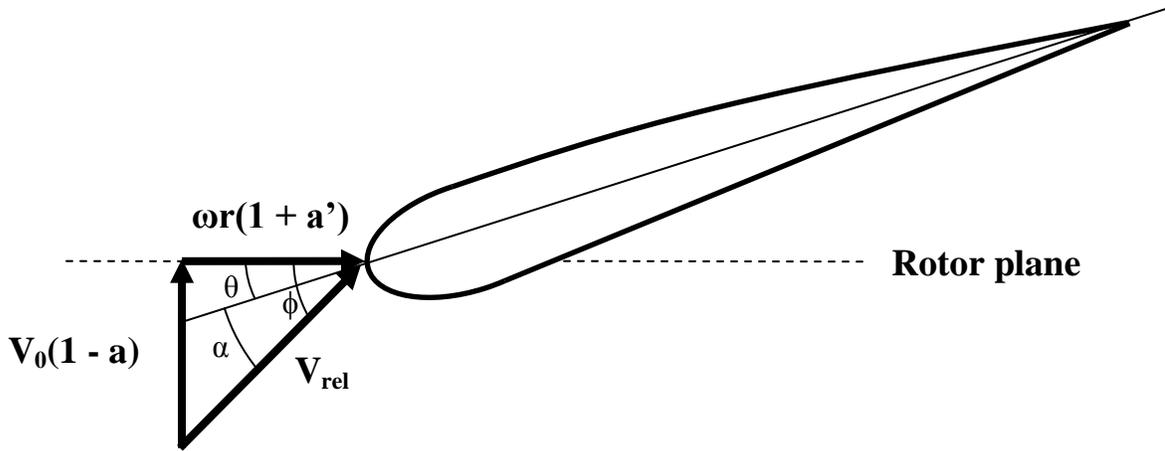
Figure 7. Velocity diagram for wind turbine blade cross-section.

where   ω   is the rotational speed of the turbine blade,

             r   is the distance from the cross-section to the centre of the hub,

             V_0 is the oncoming wind speed, corresponding to U_j in Equation 28,

             a and a'   are induction factors which are functions of the blade geometry and wind speed,

V_{rel} is the resultant effective wind speed,

ϕ is the angle between the resultant wind speed and the rotor

plane,

θ is the blade pitch, the angle between the chord line of the

blade and the rotor plane, and

α is the angle of attack of the resultant wind.

The resultant effective wind speed, V_{rel}, is equal to

$$V_{rel} = \sqrt{V_0^2(1-a)^2 + \omega^2 r^2 (1+a')^2} \qquad (29)$$

where all variables are as previously defined. The forces imparted to the blade are shown in Figure 8.
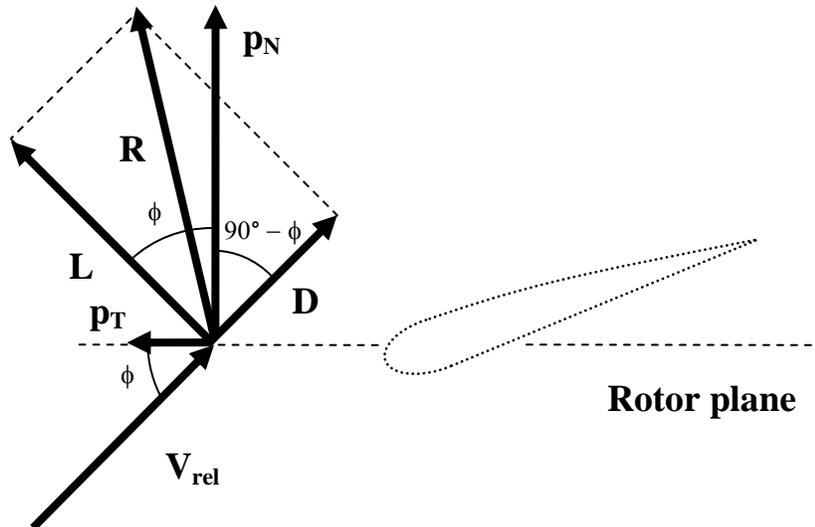
Figure 8. Force diagram for wind turbine blade cross-section.

where   L   is the lift force per unit length,

D   is the drag force per unit length,

R   is the resultant force per unit length,

p_N is the along-wind or normal force per unit length, and

p_T is the tangential force per unit length.

The magnitudes of the axial and tangential forces per unit length are given by

$$p_N = 0.5\rho V_{rel}^2 C_N c \tag{30}$$

$$p_T = 0.5\rho V_{rel}^2 C_T c \tag{31}$$

where ρ is the mass density of air,

c   is the chord length of the blade,

C_N is the along-wind or normal force coefficient, and

C_T is the tangential force coefficient.

The force coefficients are calculated as

$$C_N = C_L\cos\varphi + C_D\sin\varphi \tag{32}$$

$$C_T = C_L\sin\varphi - C_D\cos\varphi \tag{33}$$

where C_L is the lift coefficient of the blade section, and

C_D is the drag coefficient of the blade section.

These force coefficients can be determined from the geometry shown in Figure 8, and result from resolving the lift and drag force vectors into along-wind and tangential force vectors.

The preceding equations can be used to generate a set of coherent wind time histories and calculate the corresponding loads on the turbine blades and tower. The turbulence properties described by Equations 11 to 16 are used as inputs to the numerical scheme described in Equations 17 to 28 to generate a set of coherent wind speed time-histories. The time-histories are then transformed, using Equations 29 to 33, to loading time-histories on the blades. For the tower, the time-histories are applied as in Equation 9.

The velocity of the structure in the along-wind direction must be subtracted from the oncoming wind speed to yield the effective wind speed applied to the structure. The effective wind speed is increased as the structure moves in the direction opposite the wind and decreased as the structure moves in the same direction as the wind. This effect is known as aerodynamic damping, and can be captured by subtracting the structural velocity from the wind velocity in Equation 9, and from the effective wind velocity V_0 shown in Figure 7.

3.2.2 Seismic Loading

Seismic loading is applied to a structure through ground acceleration, primarily in the lateral direction, although in some cases the vertical component of ground motion is of interest. The mass of a structure gives rise to inertial loading due to ground acceleration. For horizontal ground acceleration, the force applied to the structure is

$$F_{seismic} = -m(x, y, z)\ddot{x}_g \tag{34}$$

where   m   is the spatial mass distribution of the structure, and

              $\ddot{x}_g$ is the ground acceleration.

There are two main methods of evaluating seismic loads on a structure: response spectrum analysis (RSA) and response history analysis (RHA). RSA is commonly used for typical building and bridge structures where the response is governed by a few dominant modes, while RHA is used for flexible and/or non-linear dynamically sensitive structures.

In RSA, the natural frequencies and modes of the structure are calculated and the vibration modes are treated as individual single degree of freedom oscillators. The peak response of the structure in a number of consecutive modes is determined from a response spectrum based on local ground conditions and the peak responses are combined to estimate the peak total response of the structure. The number of modes required depends on the nature of the structure and the applied loads as well as the degree of accuracy required. In RHA, which is valid for wind loading as well as seismic loading, the dynamic equations of motion are formed and solved for some time-history of loading. This loading may be synthetically generated or based on measurements. The details of both RSA and RHA have been extensively documented in standard structural dynamics texts (e.g. Craig, 2006). For this thesis, response history analysis is used due to the dynamic sensitivity of the structure and the non-linearity introduced by blade rotation and vibration isolation.

3.3 Vibration Isolator Idealization

The vibration isolator acts to couple the tower to the nacelle-hub-rotor assembly. For this investigation, the vibration isolator is idealized as a linear elastic spring, a linear viscous damper, and a hysteretic element in parallel. A schematic of this idealization is shown below:

Linear Elastic Element

Linear Viscous Element

Top of Tower

Bottom of Nacelle

Hysteretic Element
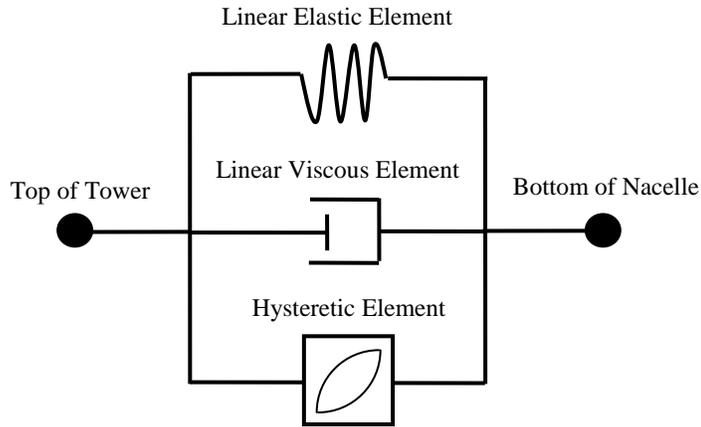
Figure 9. Schematic of vibration isolator.

The motion of a single degree of freedom (SDOF) oscillator with linear viscous damping and Bouc-Wen hysteresis is governed by the equation (Ismail, 2009):

$$m\ddot{x} + c\dot{x} + F_r(t) = f(t) \tag{35}$$

where   m   is the mass of the SDOF oscillator,

           c   is the linear viscous damping coefficient,

           $\ddot{x}$ is the oscillator acceleration,

           $\dot{x}$ is the oscillator velocity,

           $F_r(t)$ is the restoring force, and

$$f(t) \qquad \text{is the externally applied load.}$$

The restoring force is expressed as

$$F_r(t) = ak_ix + (1-a)k_iz \qquad (36)$$

where k_i is the initial stiffness of the system,

           a is the ratio of the post-yield stiffness to the initial stiffness,

           x is the oscillator displacement, and

           z is the hysteretic displacement.

The restoring force contains an elastic component, defined by the first term of the equation, and a hysteretic component, defined by the second term of the equation. Thus, the restoring force can be thought of physically as a linear spring and a non-linear spring in parallel. The hysteretic displacement is defined as the solution to a first-order non-linear differential equation having zero initial condition (Ismail, 2009), given by

$$\dot{z} = \dot{x}\{A - [B * \mathrm{sign}(z\dot{x}) + \gamma]|z|^n\} \qquad (37)$$

where $\dot{z}$ is the hysteretic velocity, and

           A, β, γ, n are parameters defining the hysteretic behaviour.

For an isolator which is flexible in both lateral directions, corresponding versions of Equations 35 and 36 can be written for each direction. Assuming $n = 2$, the bidirectionally coupled

hysteretic displacements are defined by the equations having zero initial condition (Narasimhan, 2006), given by

$$\dot{z}_x = \dot{x}\{A - [B * \text{sign}(z_x \dot{x}) + \gamma]z_x^2\} - \dot{y}\{[B * \text{sign}(z_y \dot{y}) + \gamma]z_x z_y\} \tag{38}$$

$$\dot{z}_y = \dot{y}\{A - [B * \text{sign}(z_y \dot{y}) + \gamma]z_y^2\} - \dot{x}\{[B * \text{sign}(z_x \dot{x}) + \gamma]z_x z_y\} \tag{39}$$

where z_x, z_y are hysteretic displacements in the x and y directions, and

x, y are physical displacements in the x and y directions.

For the Bouc-Wen model to exhibit bilinear hystereric behaviour, the parameters are constrained such that (Marano, 2007)

$$A = 1 \tag{40}$$

$$\beta = \gamma \tag{41}$$

$$x_y = \left(\frac{1}{\beta + \gamma}\right)^{\frac{1}{n}} \tag{42}$$

where x_y is the yield displacement of the isolator.

A plot of the force-displacement behaviour for a Bouc-Wen oscillator with parameters n = 2 and a = 0.1 is shown in Figure 10.
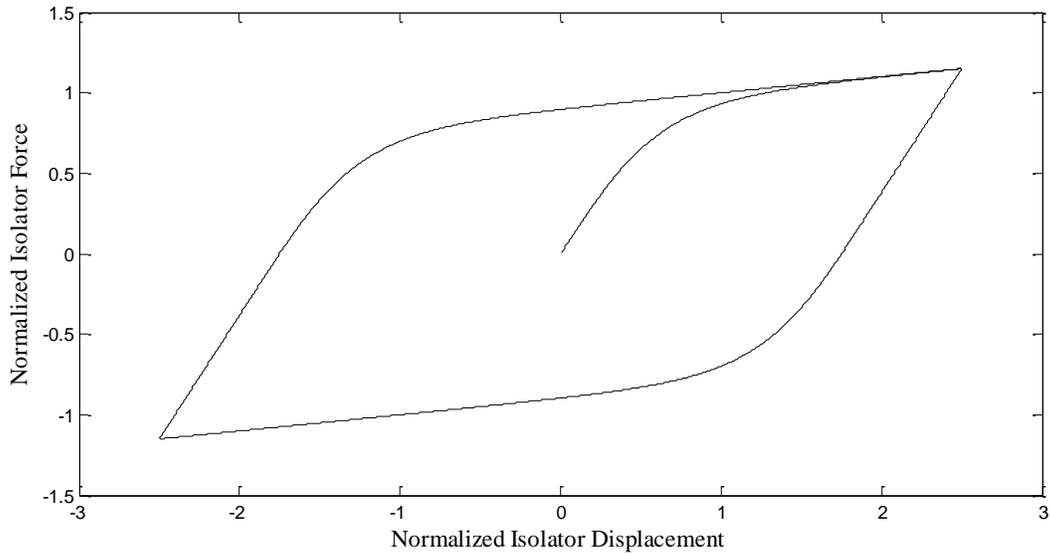
Figure 10. Normalized isolator force versus normalized isolator displacement.

The isolator displacement is normalized by the yield displacement, and the isolator force is normalized by the product of the initial stiffness and the yield displacement. The bilinear isolator has a high initial stiffness and a low post-yield stiffness. The high initial stiffness is beneficial for resisting loads below the extreme level with relatively little displacement.

Assuming that the mass of the isolator is negligible, the total force applied by the isolator in the x-direction is

$$F_{iso} = ak_i(x_{top} - x_{bottom}) + c(\dot{x}_{top} - \dot{x}_{bottom}) + (1 - a)k_iz_x \tag{43}$$

where top and bottom denote the displacements and velocities at the top and bottom of the isolator.

The displacements and forces described by Equation 43 are shown in Figure 11.
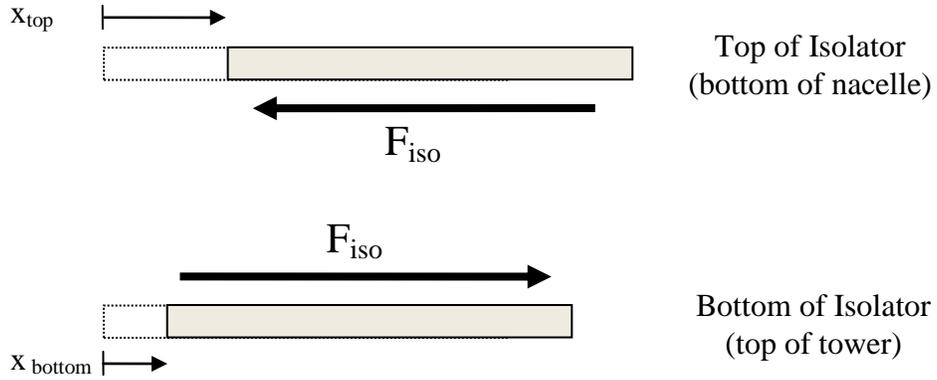
Figure 11. Isolator displacements and forces.

As shown in Figure 11, the isolator force acts to oppose differential motion between the top and bottom of the isolator. The dotted lines in the figure represent the undeformed position of the top and bottom of the isolator.

In matrix form, the forces applied at the top and bottom of the isolator in the x-direction are

$$\mathbf{F_{iso}} = \mathbf{K_{iso}}\mathbf{x_{iso}} + \mathbf{C_{iso}}\mathbf{\dot{x}_{iso}} + \mathbf{H_{iso}}z_x \tag{44}$$

where $\mathbf{F_{iso}}$ is a vector containing the forces applied at the top and bottom of the isolator,

$\mathbf{K_{iso}}$ is the isolator stiffness matrix,

$\mathbf{C_{iso}}$ is the isolator damping matrix,

$\mathbf{H_{iso}}$ is the isolator hysteretic matrix,

$\mathbf{x_{iso}}$ is a vector containing the displacements at the top and bottom of the isolator, and

z_x is the hysteretic displacement in the x-direction.

The isolator matrices are defined as

$$\mathbf{K_{iso}} = ak_i \begin{bmatrix} 1 & -1 \\ -1 & 1 \end{bmatrix} \tag{45}$$

$$\mathbf{C_{iso}} = c \begin{bmatrix} 1 & -1 \\ -1 & 1 \end{bmatrix} \tag{46}$$

$$\mathbf{H_{iso}} = (1-a)k_i \begin{Bmatrix} 1 \\ -1 \end{Bmatrix} \tag{47}$$

The isolator matrices can be used to couple the matrices described by Equation 1 for the portions of the structure above and below the isolator. The isolator stiffness and damping matrices can be assembled directly into the global stiffness and damping matrices, while the hysteretic matrix and displacement must be treated separately, and contribute non-linearly to the differential equations of motion.

The isolator natural period can be defined as the natural period that would be dominant if the isolator was the only flexible element in the structure and did not yield. The isolator natural period is equal to

$$T_{iso} = 2\pi \sqrt{\frac{M_{iso}}{k_i}} \tag{48}$$

where M_{iso} is the total mass located above the isolator.

For an isolator which has damping and yielding forces, the actual natural period is elongated. Since both the tower and blades of a wind turbine are flexible, the actual natural period of the structure will not be equal to the isolator value, but as the isolator stiffness decreases relative to

36

the stiffness of the tower and blades, the first natural period of the structure will approach the isolator natural period.

Similarly, the isolator damping coefficient can be defined as the damping coefficient that would produce a given damping ratio if the isolator was the only flexible element in the structure and did not yield. The isolator damping coefficient is equal to

$$C_i = 2\zeta\sqrt{k_i M_{iso}} \tag{49}$$

where ζ is the target damping ratio of the isolator.

The damping coefficient may also be calculated based on the post-yield stiffness, in order to avoid unrealistically high damping forces in the post-elastic range (Hall, 2006). In that case, the isolator damping coefficient is equal to

$$C_i = 2\zeta\sqrt{ak_i M_{iso}} \tag{50}$$

where the variables are as previously defined.

The behaviour of the vibration isolator can be described in detail using the information given above. Implementing the relationships described using commercial software will be discussed in the next section.

3.4 Implementation of Numerical Models

The theoretical descriptions of wind turbine structures, loading and vibration isolation in the preceding sections are implemented using MATLAB and COMSOL Multiphysics. MATLAB is a technical computing program, and is used mainly for simulation of wind loads and post-processing, while COMSOL is a finite element suite and is used to solve the differential equations of motion to study the behaviour of the turbine.

Due to the rotational coupling described by Equations 2 to 7 and the non-linear vibration isolator described by Equations 35 to 50, the wind turbine structure can be considered to consist of three sections: the blades and hub, the nacelle, and the tower. A finite element model is created in COMSOL which consists of three such sections, each physically separated from the others, as shown in Figure 12.
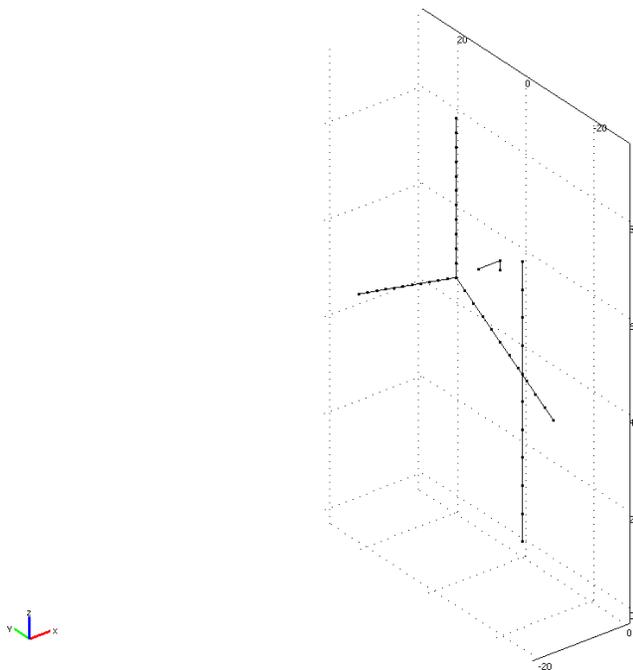
Figure 12. Geometry of COMSOL model.

In the finite element model, there is a gap between the blade-hub system and the nacelle, and between the nacelle and the tower. The equations needed to couple the three sections of the structure are written explicitly using COMSOL's capability to define global expressions. The blades, nacelle and tower are modelled using 3-dimensional frame elements, with the nacelle elements having structural properties such that they are effectively rigid. The masses of the hub and nacelle are lumped at the base of the blades and the top of the tower, respectively. The base of the tower is specified as a fixed support. The tower and blades are each separated into 10 frame elements having varied structural properties and loading, in order to capture the effects of varied structural geometry and turbulent wind loading.

The rotational coupling between the blade-hub system and the nacelle is accomplished by defining a time-dependent rotating coordinate system. The displacements and rotations at the tip of the nacelle are constrained to be equal to those at the base of the blades, appropriately transformed by the rotating coordinate system, as in Equations 2 to 7. The effects of centrifugal stiffening are incorporated using an approximate method in which the fundamental frequency of a rotating blade is calculated using MATLAB and a multiplier proportional to the centrifugal tension is applied to the elastic modulus of the blades in the finite element model to match that natural frequency. Typically, the stiffening would be modelled using a tension-dependent geometric stiffness matrix, which is described in numerous structural analysis texts (e.g. Weaver, 1980). However, the approximate method described above was necessary because COMSOL does not incorporate geometric stiffness for frame elements.

Turbulent wind speeds are simulated in MATLAB using the method described in Equations 9 to 28. The calculated wind speeds are input into COMSOL as functions. COMSOL allows for the calculation of distinct local properties for each frame element. Each frame element is assigned a

numeric index to identify which wind speed time history is applied to it. The structural and aerodynamic properties described by Equations 29 to 33 are calculated for each blade segment, then used to determine the along-wind and tangential loading on that segment. The loads calculated for both the tower and blades are then applied to the structure. Records of seismic ground acceleration are also input into COMSOL as functions. The ground accelerations are multiplied by the mass of the structure and applied as loads to the frame members as well as the lumped masses at the hub and nacelle.

The vibration isolator is implemented in COMSOL by adding the differential equations for the hysteretic displacement as global equations to be solved alongside the equations of motion. The hysteretic displacements are solved simultaneously with the equations of motion and are used in global equations to calculate the forces applied by the isolator. These forces are applied to the structure at the nodes corresponding to the top and bottom of the isolator.

COMSOL solves the equations of motion in the time domain rather than using modal analysis. This solution method is well-suited to a non-linear problem such as a wind turbine with blade rotation and vibration isolation. However, solving non-linear structural problems in the time domain requires care in ensuring that the solution is accurate and stable. In most cases, a significantly smaller time-step is required when solving a non-linear problem in the time domain compared to solving a linear problem in either the time domain or the modal domain. The time-step must be sufficiently small that all natural frequencies of interest can be resolved, and small enough that the solution will not exhibit instabilities. Choosing such a time-step requires studies of convergence and iteration, which were performed at the beginning of this investigation.

Two solvers are available in COMSOL for time-dependent problems, the generalized-alpha solver and the BDF solver. Both solvers involve the use of numerical damping to provide stability to the solution. The BDF uses an implicit backward interpolation method and tends to damp higher frequencies more severely than the generalized-alpha solver. The BDF solver is thus more stable than the generalized-alpha solver but also dissipates higher frequencies more strongly (COMSOL, 2011). Using a time-step of 0.001 s, the BDF solver was found to be stable and accurate for simulations including both blade rotation and vibration isolation, while the generalized-alpha solver was unable to achieve convergence. The sampling frequency associated with this time step is far higher than the structural frequencies of interest, which are generally below 10 Hz. The BDF solver was used for all simulations.

The numerical idealization described in this chapter is assigned physical properties and used to perform a parametric study of the behaviour of the full turbine system under wind and seismic loading.

4. Example Turbine and Simulation Regime

This chapter discusses the properties of the turbine under consideration, the seismic and wind loading applied to the turbine, and the key variables being considered to evaluate the effectiveness of the vibration isolator.

4.1 Example Turbine

The properties of the wind turbine used in this study are based on general information regarding utility-class turbine structures culled from published sources (e.g. Hansen, 2008; Burton, 2001). This design is not necessarily representative of any specific wind turbine structure. Its purpose, thus, is not to demonstrate the exact structural response that a typical turbine would exhibit under the applied loading but to demonstrate the potential change in structural response that could be realized by the use of a vibration isolator. This is accomplished by reporting the structural response in the form of normalized response variables rather than dimensional response quantities.

4.1.1 Turbine Structural and Aerodynamic Properties

The turbine has a hub height of 60 m. The tower is a cylindrical steel shell with outside diameter of 3.8 m at its base, tapering linearly to 2.3 m at hub height. The wall thickness of the tower is 35 mm for its entire height. The tower steel has a Young's modulus of 210 GPa, Poisson's ratio of 0.3, and mass density of 7850 kg/m^3. The tower has a drag coefficient of 1.2 which is

representative for a cylindrical structure. The base of the tower is assumed to be a fixed connection. Soil-structure interaction is neglected.

The blades are hollow rectangular sections with outside width of 3 m normal to the along-wind direction at their bases, tapering linearly to 1.5 m at their ends. The outside depth of the blades is 0.8 m parallel to the along-wind direction, and the wall thickness is 15 mm. The blades have a Young's modulus of 65 GPa, Poisson's ratio of 0.2, and mass density of 2100 kg/m^3. The blades are 30 m long with a hub radius of 3 m, for a total length of 33 m from the centre of the hub to the tip of the blade. The pitch angle of the blades, denoted by θ in Figure 7, tapers linearly from 0.2 radians at the base of the blades to zero at the tip of the blades.

Near the tip of the blades, the effective wind speed associated with blade rotation is significantly higher than the oncoming wind speed. The increased resultant wind speed leads to high structural forces imposed on the blade. The tangential forces cause the blades to rotate and generate power, while the along-wind forces are resisted by the structure but do not contribute to power generation. Induction factors a and a', shown in Figure 7, are assumed to be equal to zero so that the resultant wind speed is calculated directly using the oncoming wind speed.

The relationship between the angle of attack of the wind and the lift and drag coefficients is chosen based on previously discussed literature. It is assumed that the lift coefficient is defined at a number of points, as given in Table 1.

Table 1. Discrete Values of Lift Coefficient

Angle of Attack (degrees)	Lift Coefficient
0	0.0
10	1.0
25	0.75
40	1.0
90	0.0

At intermediate angles of attack, linear interpolation is used. The drag coefficient is assumed to be a continuous sinusoidally varying function of the angle of attack, equal to a minimum of zero at a $0°$ angle of attack and a maximum of 1.8 at a $90°$ angle of attack. The mass density of air is assumed to be 1.25 kg/m^3. The mass of the hub is assumed to be 20000 kg and the mass of the nacelle is assumed to be 50000 kg. These masses are lumped at the base of the blades and the top of the tower, respectively.

Damping is assumed to be 1% of critical for both the tower and the blades. Rayleigh damping is implemented for the blades based on their uncoupled natural frequencies and implemented for the tower based on the tower bending frequencies of the parked turbine structure.

Centrifugal stiffening of the blades, as described previously, is implemented using an approximated modification to the elastic modulus of the blades. For an assumed rotational period of 3.5 seconds, the increase in the elastic modulus at the base is approximately 6%, and results in an increase of 2.5% in the fundamental frequency of the blade. Aerodynamic damping is incorporated explicitly in COMSOL by subtracting the structural velocity from the velocity of the oncoming wind.

Descriptions and properties of the first few natural modes of the un-isolated structure which participate in the along-wind response are shown in Table 2.

Table 2. Properties of Un-isolated Turbine Natural Modes

Natural Frequency (Hz)	Description	Modal Participating Mass Ratio
0.567	Along-wind tower bending	63.2%
1.413	Along-wind blade bending	1.9%
1.536	Along-wind blade bending	1.4%
3.606	Tower and blade bending	2.6%
4.201	Tower and blade bending	12.7%

Images of the vibration modes in Table 2 can be found in Appendix A. As shown in Table 2, vibration in the along-wind direction includes contributions from a number of distinct modes. The total mass participation in the along-wind direction for the modes shown is 81.8%, less than the 85% typically specified in codes. The fact that the along-wind mass participation is spread across a number of modes makes time-domain solution, as performed in COMSOL, an appropriate solution method even for the case where the turbine is parked with no isolator and has a linear response which would be amenable to modal solution.

4.1.2 Vibration Isolator Properties

The vibration isolator is implemented as a bi-directionally coupled Bouc-Wen model. Displacement of the isolator in the global x and y directions is allowed, while the isolator is assumed to be rigid in the global z direction and with respect to rotation about all three directional axes. The vertical distance from hub height to the isolator is assumed be 2 m. The height of the isolator is neglected for this study.

The isolator is defined by its yield displacement, initial stiffness, ratio of initial to post-yield stiffness, and damping coefficient. The isolator properties are selected to minimize yielding

under operational wind loading but to allow some yielding during seismic events. To achieve these objectives, it is necessary to have either a high initial stiffness or a high yield displacement. Based on practical considerations, a yield displacement of 50 mm is used. The initial stiffness is varied from 1500 kN/m to 15000 kN/m in steps of 1500 kN/m, for both seismic and wind loading. Assuming a stiffness ratio of 0.1, the lower bound, 1500 kN/m, has a post-yield stiffness of 150 kN/m, which gives an equivalent post-yield isolator natural period of 4.1 seconds, well above the characteristic natural periods of most seismic events. The upper bound is an order of magnitude greater than the lower bound. For one representative value of initial stiffness, damping ratios of 0, 5%, 10%, 15% and 20% based on the post-yield stiffness are considered under seismic loading, to quantify the effects of damping.

4.1.3 Key Response Variables

The effectiveness of vibration isolation is quantified by comparing the response of the isolated turbine to that of the un-isolated turbine. For this study, based on the literature discussed, the primary response quantities of interest are structural actions, such as base shears and bending moments in the tower and blades; structural displacements; and structural accelerations. For strength design, it is important to study the peak values of the response. As well, it is useful to know the standard deviation of the response for evaluating concerns such as reliability, availability, and fatigue life. The locations on the structure at which the structural responses are evaluated are shown in Figure 13.
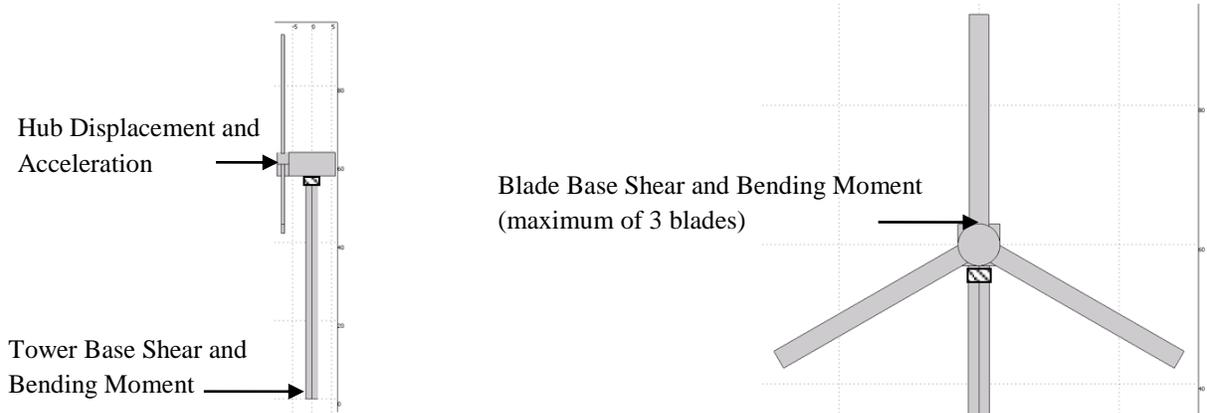
Figure 13. Locations of key response variables

The key response variables considered for the isolated turbine structure can be written formally as

$$J_1 = \text{normalized hub displacement} = \frac{\text{alongwind hub displacement}}{\text{unisolated alongwind hub displacement}}$$

$$J_2 = \text{normalized hub acceleration} = \frac{\text{alongwind hub acceleration}}{\text{unisolated alongwind hub acceleration}}$$

$$J_3 = \text{normalized tower base shear} = \frac{\text{tower base shear}}{\text{unisolated tower base shear}}$$

$$J_4 = \text{normalized tower base moment} = \frac{\text{tower base moment}}{\text{unisolated tower base moment}}$$

$$J_5 = \text{normalized blade base shear} = \frac{\text{alongwind blade base shear}}{\text{unisolated alongwind blade base shear}}$$

$$J_6 = \text{normalized blade base moment} = \frac{\text{alongwind blade base moment}}{\text{unisolated alongwind blade base moment}}$$

Each of these key response variables consists of a response value for the turbine with a vibration isolator, normalized by the corresponding response value of the turbine without a vibration isolator.

47

Objective functions can be defined in order to compare the performance of varied isolator configurations. Objective functions used in the study are defined as

$$O_1 = \text{kinematic objective function} = \frac{J_1^2 + J_2^2}{2}$$

$$O_2 = \text{tower response objective function} = \frac{J_3^2 + J_4^2}{2}$$

$$O_3 = \text{blade response objective function} = \frac{J_5^2 + J_6^2}{2}$$

The isolator properties which minimize a given objective function can be considered to be the optimal parameters with respect to the corresponding response variables. The objective functions were selected such that if both of the response parameters considered were equal to 1, indicating no change in structural response, the objective function would also be equal to 1.

Two additional key response variables can be defined for the isolator itself, namely the peak isolator force and the peak displacement across the isolator. Normalized versions of these variables can be written as

$$J_7 = \text{normalized isolator force} = \frac{\text{isolator force}}{\text{isolator yield force}}$$

$$J_8 = \text{normalized isolator displacement} = \frac{\text{displacement across isolator}}{\text{isolator yield displacement}}$$

These variables do not have analogous values in the un-isolated structure, and thus they are used to characterize the isolator itself rather than its effect on the turbine structure.

4.2 Simulation Regime

The performance of the wind turbine with and without the vibration isolator is assessed under wind and seismic loading in the along-wind direction. The simulations are performed using the finite element model previously discussed. The simulation conditions are discussed in this section.

4.2.1 Seismic Loading

As previously discussed, seismic analysis may be carried out using response spectrum (RSA) or response history (RHA) methods. For this study, RHA is used due to the non-linearity and dynamic sensitivity of the structure. Recordings of three well-known ground motions from the 1994 Northridge earthquake in California, USA are used to study the seismic response of the wind turbine. The Northridge earthquake took place January 17, 1994. It caused extensive structural damage to many buildings, highways and bridges, and lead to significant changes in building standards and enforcement.

Records of ground motions in the Northridge earthquake were retrieved from the NGA Database of the Pacific Earthquake Engineering Research (PEER) Centre at the University of California. Key information for the three ground motion records studied is shown in Table 3.

Table 3. Key Information for Seismic Records

Short Name	Location	Selected Component	Peak Ground Acceleration	Sampling Rate
Newhall	Los Angeles County Fire Station	NWH360	0.59 g	50 Hz
Rinaldi	Rinaldi Receiving Station	RRS228	0.83 g	100 Hz
Sylmar	Sylmar Convertor Station East	SCE018	0.83 g	200 Hz

Each ground acceleration record consists of two orthogonal horizontal components and a vertical component. Since this study focuses only on motion in the along-wind direction it is necessary to select a single horizontal component of each record. The designations of the components used, which can be used to locate these records in the PEER NGA online database, are noted in the table. The high values of peak acceleration demonstrate that these records represent extremely strong ground motions.

Figure 14 shows plots of the ground acceleration records.
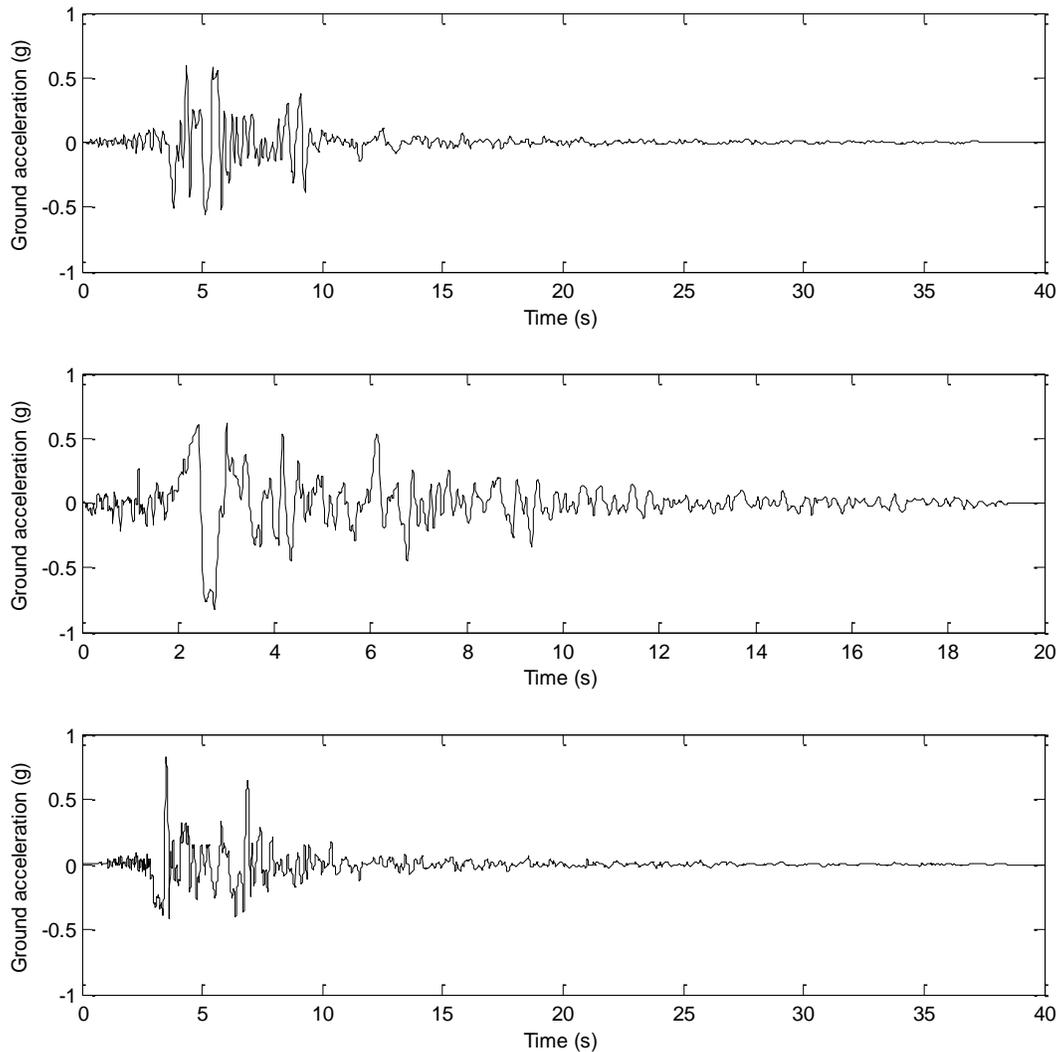
Figure 14. Ground acceleration versus time for Newhall, Rinaldi and Sylmar records.

The structural response behaviour for the seismic events demonstrates the effect of the vibration isolator under a high-frequency time-varying load which is essentially zero-mean. The values of the peaks and standard deviations of the key response variables are calculated over the first 20 seconds of each seismic event, which corresponds to the time of the strongest ground acceleration. Figure 15 shows response spectra for these seismic events.

51
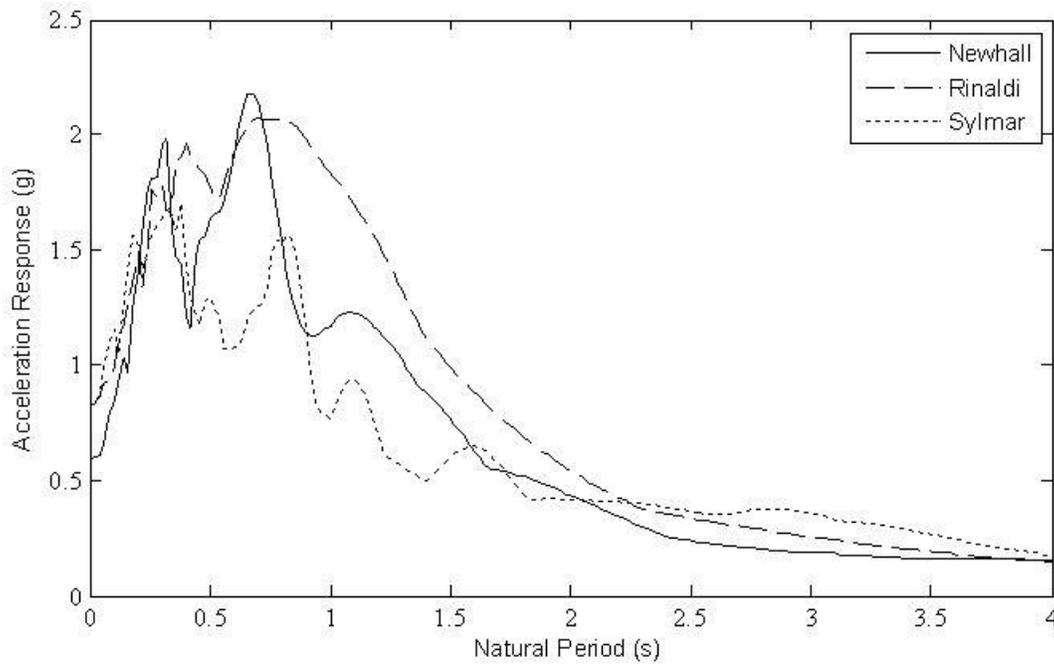
Figure 15. Acceleration response spectra for seismic events with 5% damping

The first natural period of the un-isolated structure is approximately 1.75 seconds which is above the peak response range for these seismic events. However, the natural periods involving significant blade bending are in the range of 0.7 seconds, at which the dynamic response may be significant.

It is noted that for a detailed structural design, the use of only three single-component ground acceleration time histories would not be sufficient to characterize extreme loading conditions, and that the ground accelerations would need to be scaled to take into account local seismic hazard and site conditions. The key response variables should not be considered to be peak values for design but as values for evaluating the effectiveness of the isolator.

For the seismic loading simulations, the turbine is assumed to be in a parked position with one blade in the vertical position.

4.2.2 Wind Loading

As discussed previously, IEC 61400-1 presents turbulent wind models as well as deterministic loading cases to be considered for wind turbine design. For this study, the deterministic loading cases are not considered; a simulation of turbulent wind is generated and applied to investigate the behaviour of the isolated turbine under wind loading. For wind loading, the turbine is assumed to be in operation with a rotational period of 3.5 s.

The Normal Turbulence Model (NTM) from IEC 61400-1 is used to simulate the wind loading. An operational mean wind speed of 10 m/s is assumed with a standard deviation of 1.8 m/s calculated from IEC 61400-1. The length scale at hub height for wind speed simulation is determined to be 340 m. These inputs are used along with the PSD and coherence functions to carry out the numerical scheme summarized in Equations 17 to 28 to generate a grid of coherent wind time histories using MATLAB; the program used to do so is provided in Appendix C.

Wind speed time-histories are simulated and applied to both the blades and the tower. Wind time-histories are simulated at ten points along the height of the tower and applied as uniform loads to segments of the tower. The wind loading on the tower is multiplied by a power-law profile as in Equation 10. The wind time histories for the blades are simulated in a radial grid, similar to that shown in Figure 16.
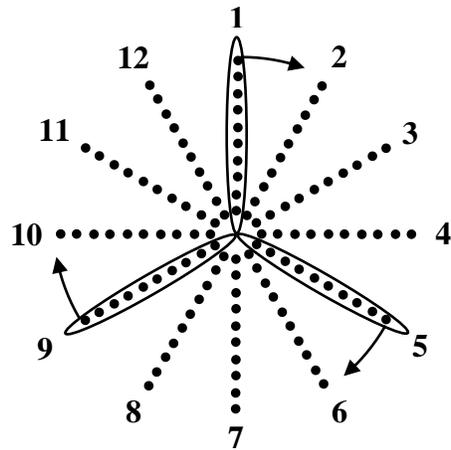
Figure 16. Locations of wind simulation points for blades.

Wind speed time-histories are simulated in 12 radial lines, with 10 time-histories simulated along each line. As the blades rotate, the fixed point whose wind speed is applied to the blade changes with time as the blade sweeps through each radial line

The set of wind speed time-histories has a length of 40 seconds and sampling rate of 20 Hz, corresponding to a frequency range for the turbulent wind of 0.025 Hz to 10 Hz. This range contains excitations at the natural frequencies of interest.

To avoid the strong transients that are induced by introducing sudden wind loading to a structure initially at rest, the wind speed time-histories are scaled such that the mean wind speed increases linearly from zero to 10 m/s over the first 10 seconds of the simulation. A sample wind speed time history can be seen in Figure 17.
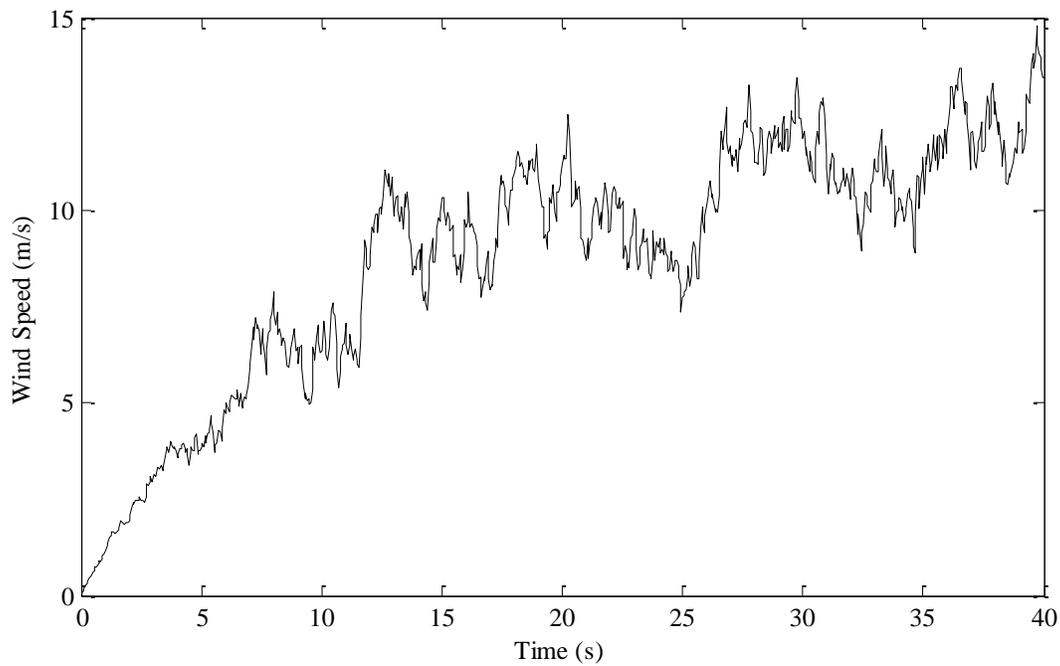
Figure 17. Sample wind speed time history.

As shown, the wind speed increases approximately linearly from zero to 10 seconds. The peaks and standard deviations of the key variables, for the wind loading cases, are calculated over the 30-second period between 10 and 40 seconds, to approximate a reasonably steady-state response.

For structural design, the use of many sets of synthetic wind time histories would be required, using statistical analysis to extrapolate the calculated responses to those random excitations. A single set of wind speeds is used in this study, to provide a demonstration of the behaviour of the turbine under wind loading.

4.2.3 Summary of Simulation Hierarchy

The simulation regime consists of two studies, one to investigate the effect of the vibration isolator under seismic loading and one to investigate its effect under wind loading. Prior to these studies, simulations were performed to determine the benchmark structural response of the un-isolated turbine.

The first parameter study involves varying the initial stiffness of the isolator with a constant yield displacement of 50 mm and isolator damping ratio of 5% based on post-yield stiffness, under the three seismic loading cases. For an initial stiffness value of 7500 kN/m, the damping ratio is varied from 0 to 20% based on post-yield stiffness, under the three seismic loading cases. This study is performed with the turbine in the parked position with one blade vertical.

The second study involves varying the initial stiffness of the isolator with a constant yield displacement of 50 mm and isolator damping ratio of 5% based on the initial stiffness for a single case of wind loading. This study is performed assuming the turbine blades are rotating with a period of 3.5 seconds.

5. Results of Simulations

This chapter summarizes the results of studies carried out to investigate the structural response of the example turbine under seismic loading and under wind loading with varied vibration isolator properties.

5.1 Structural Response under Seismic Loading

The un-isolated and isolated turbine structures are subjected to seismic loading to investigate the effects of varying the initial isolator stiffness, and of varying the degree of isolator damping. The results are presented in this section.

5.1.1 Effects of Varied Isolator Stiffness

The un-isolated and isolated turbine structures are each subjected to the Newhall, Rinaldi and Sylmar seismic time histories. For the isolated turbine structures, a yield displacement of 50 mm is assumed. Simulations are performed using initial isolator stiffness values varying from 1500 kN/m to 15000 kN/m, with an assumed isolator damping ratio of 5% based on the post-yield stiffness. The peak values of the key response variables are shown in Figure 18.
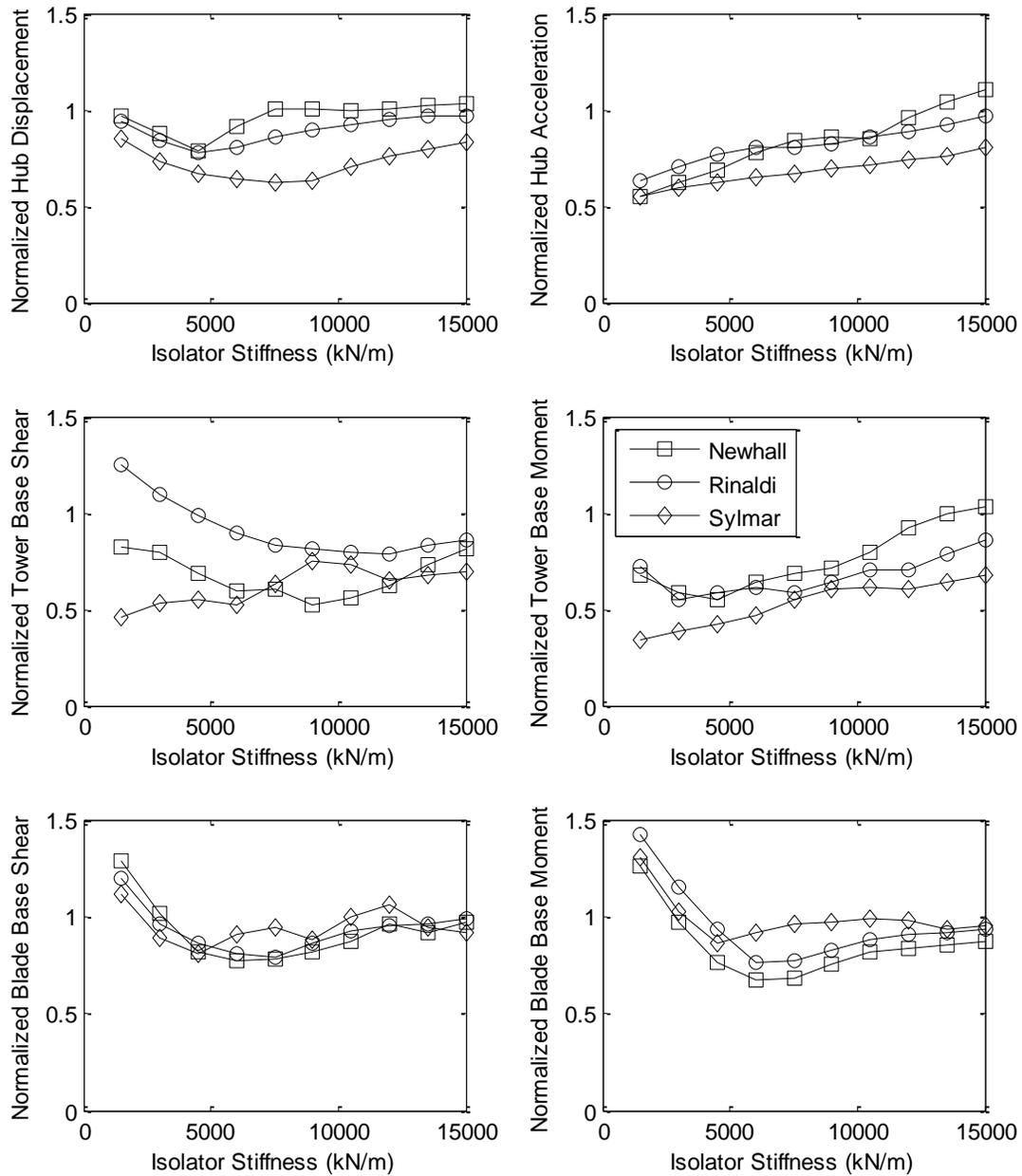
Figure 18. Peak values of key response variables under seismic loading with varied isolator stiffness.

The hub displacement of the structure is generally decreased, with a minimum value occurring at a stiffness of 4500 kN/m under the Newhall and Rinaldi excitations and at a stiffness of 6000 kN/m under the Sylmar excitation. The hub acceleration does not show a minimum, but shows a general trend of increasing as the isolator stiffness increases. Both the hub displacement and acceleration show decreases or very modest increases across the range of isolator stiffnesses.

The tower base shear shows a decrease at isolator stiffnesses above 3000 kN/m, minimum values at an isolator stiffness of 10000 kN/m for the Newhall and Rinaldi excitations and a relative maximum at the same stiffness for the Sylmar excitation. For all three excitations the tower base shear is generally reduced by the presence of the vibration isolator. The tower base moment shows a decrease at isolator stiffnesses below 12000 kN/m for all three excitations, with a general trend of increasing tower base moment with increasing isolator stiffness.

The blade base shear and blade base moment show decreases or very modest increases at isolator stiffness values above 3000 kN/m. Both variables show minimum values between isolator stiffness values of 5000 kN/m to 10000 kN/m, suggesting an optimal stiffness value in that region.

In addition to the peak values, the standard deviations of the key response variables are of interest, and are shown in Figure 19.
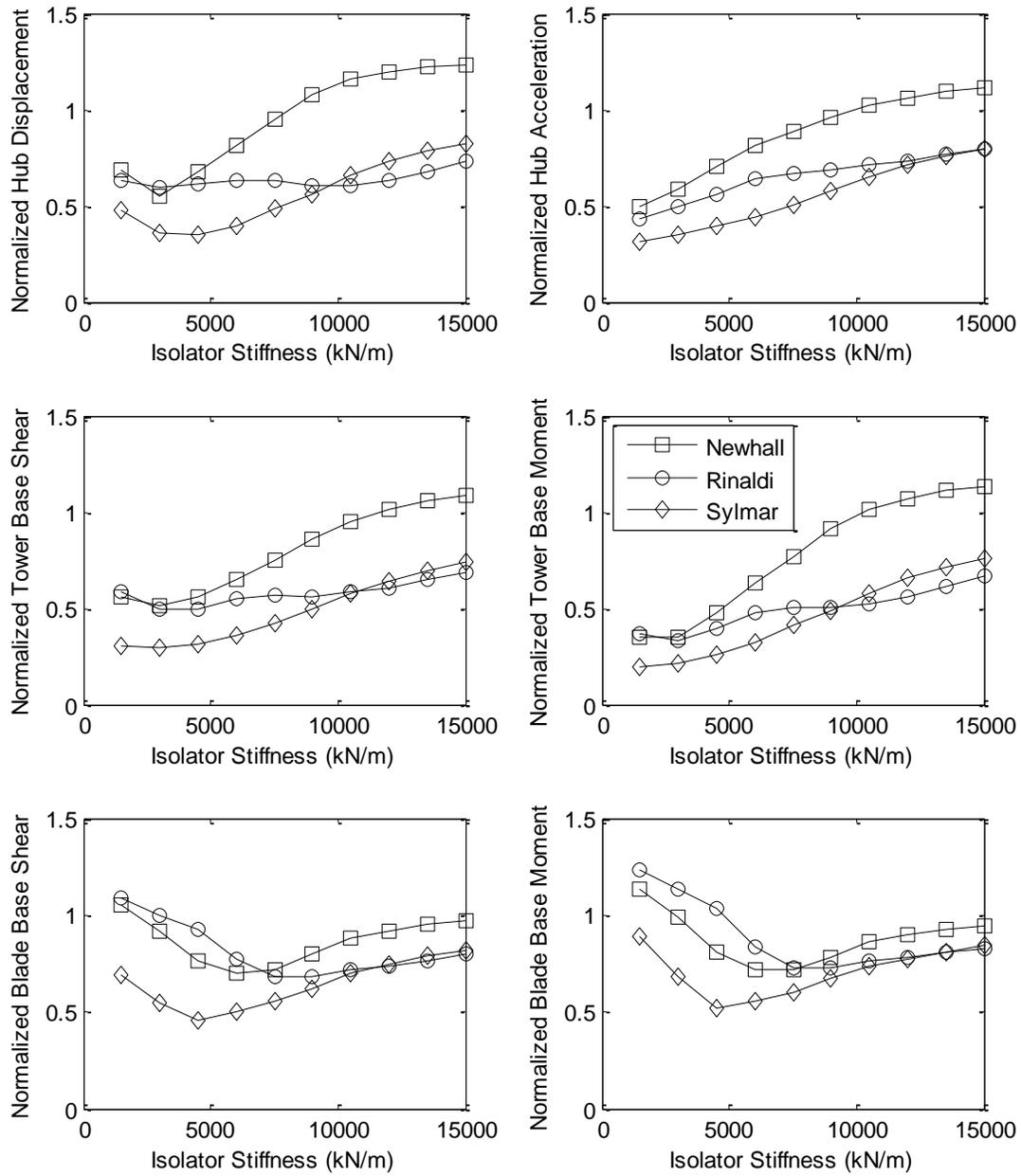
Figure 19. Standard deviation values of key response variables under seismic loading with varied isolator stiffness.

The standard deviation of the hub displacement is decreased at all values of isolator stiffness for the Rinaldi and Sylmar excitations, and at stiffnesses below approximately 7500 kN/m for the Newhall excitation. A similar trend is observed for the standard deviation of the hub acceleration.

The standard deviations of the tower base shear and tower base moment are decreased at all values of isolator stiffness for the Rinaldi and Sylmar excitations, and at stiffnesses below approximately 10000 kN/m for the Newhall excitation. No clear minimum is observed.

The standard deviations of the blade base shear and blade base moment are decreased for all three seismic excitations, at stiffnesses higher than approximately 3000 kN/m. Minimum values are observed for the standard deviations of both parameters for each seismic event. These minimum values are not identical, but generally lie between isolator stiffnesses of 5000 kN/m and 10000 kN/m.

In order to better quantify the observed minimum values, the objective functions previously defined for kinematic response, tower response, and blade response are plotted against the initial isolator stiffness. For the objective function plots, the key response variables for the three seismic events are first averaged, so that a single optimal value of isolator stiffness can be estimated. The objective functions for the peaks and standard deviations of the key response variables are shown in Figure 20.
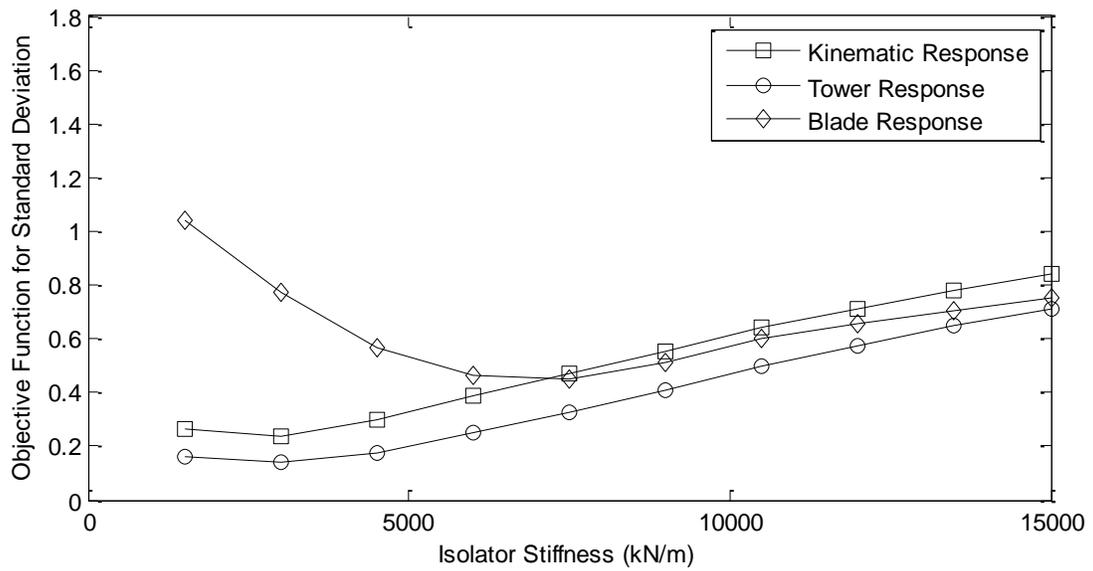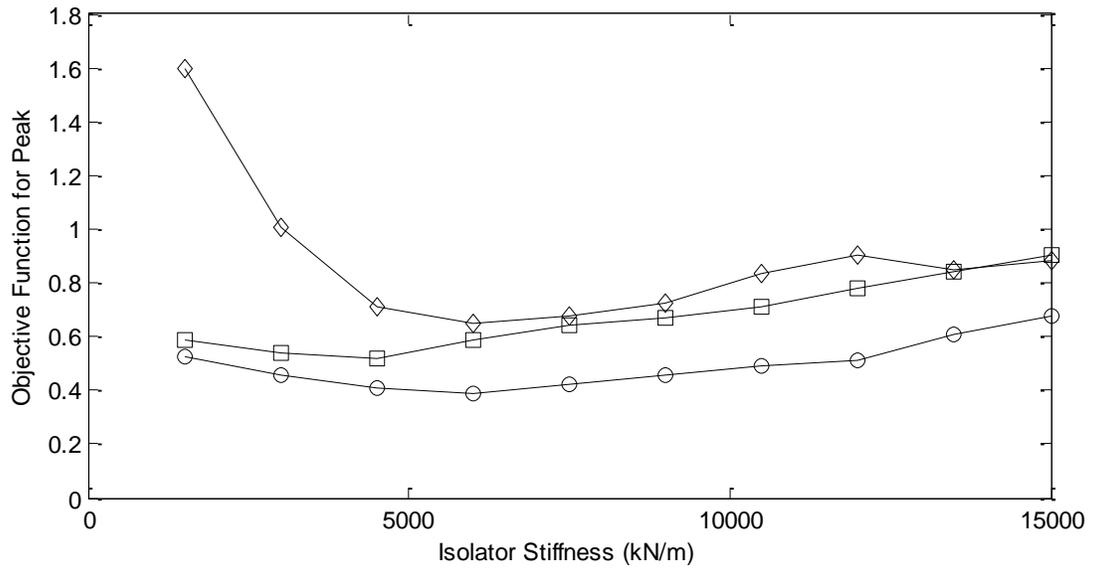
Figure 20. Objective functions for peak and standard deviation values of key response variables under averaged seismic loading with varied isolator stiffness.

The objective function for blade response shows a minimum at isolator stiffnesses between approximately 5000 kN/m and 10000 kN/m. The objective functions for the kinematic and tower responses do not show clear minimum values, but their numerical values show that the associated normalized parameters are decreased in the range of the minimum value for the blade response objective function.

Based on the response plots and the objective function plots, an initial isolator stiffness between 5000 kN/m and 10000 kN/m provides significant reductions in all key response variables under the three seismic loading cases. The numeric values of the key response variables for the three seismic excitations are found in tabular form in Appendix B.

The normalized isolator force and isolator displacement variables are also of interest. Regardless of the degree to which the key response variables of the turbine structure are reduced, isolation cannot be implemented if the isolator cannot safely sustain the peak force or displacement necessary to realize those reductions in response. The peak values of the normalized isolator displacement and normalized isolator force are shown in Figure 21.
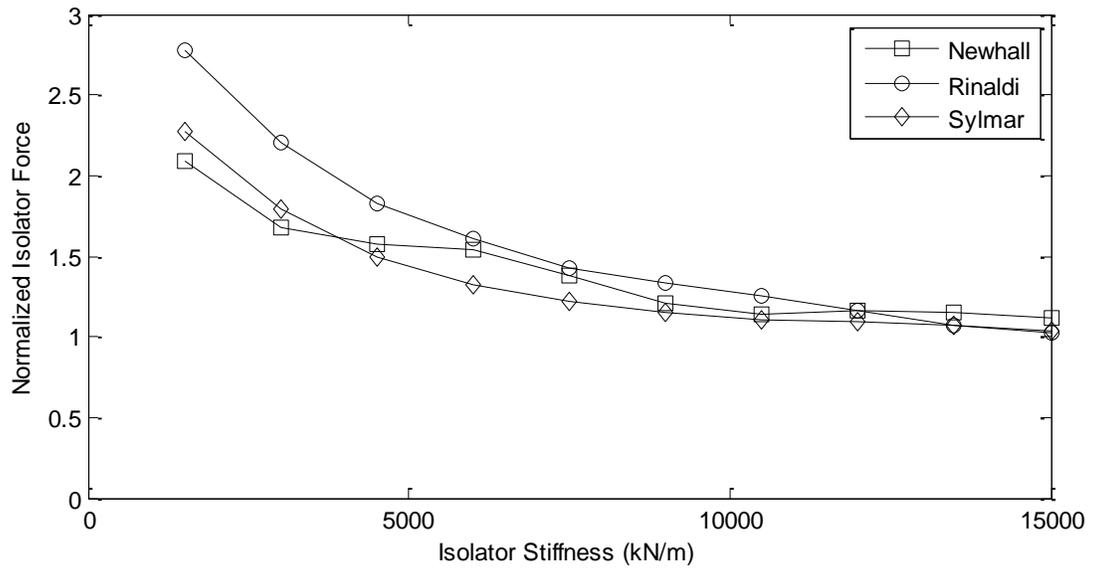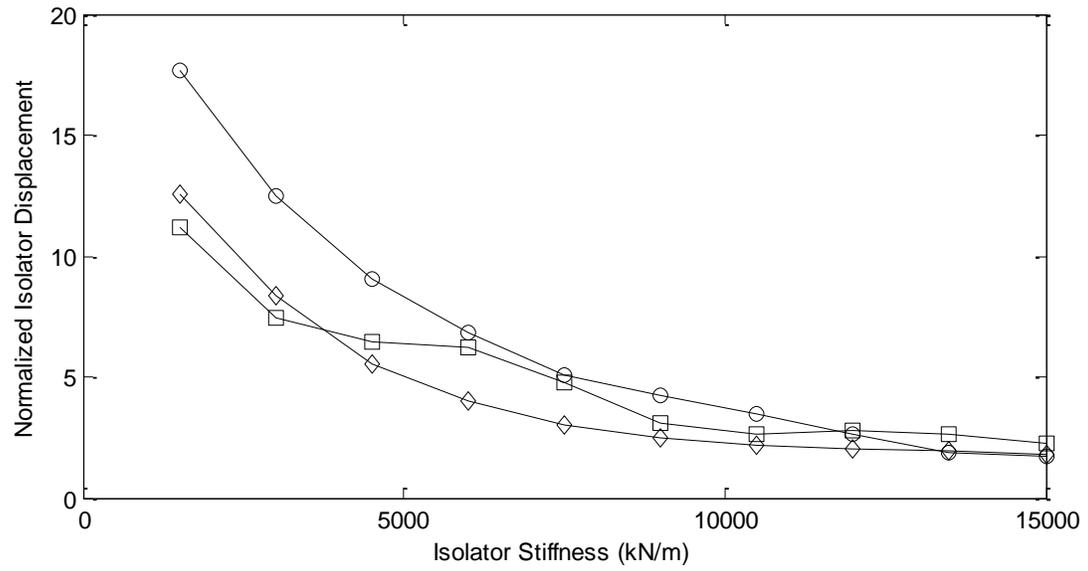
Figure 21. Peak values of isolator key response variables under seismic loading with varied isolator stiffness.

At low values of isolator stiffness, the peak values of the normalized isolator displacement are very large, indicating that the isolator displaces far past its linear elastic range. For the optimal range of 5000 kN/m to 10000 kN/m previously identified, the normalized isolator displacement ranges from approximately 3 to 6, corresponding to a peak isolator displacement between 150 mm and 300 mm. This displacement, while relatively large, can reasonably be accommodated by a properly designed isolation system.

In the same optimal range, the normalized isolator force varies from approximately 1.2 to 2. Due to the bilinear nature of the isolator, isolator displacements increase at a significantly greater rate than the corresponding isolator forces after the onset of yielding. The isolation system, when designed, must be capable of sustaining the associated isolator force without failure.

5.1.2 Effects of Varied Isolator Damping

The un-isolated and isolated turbine structures are each subjected to the Newhall, Rinaldi and Sylmar seismic time histories. For the isolated turbine structure, a yield displacement of 50 mm and an isolator stiffness of 7500 kN/m are assumed, with the damping ratio varied from 0 to 20%, based on the post-yield isolator stiffness. The peak values of the key response variables are shown in Figure 22, normalized by the peak values for zero isolator damping.
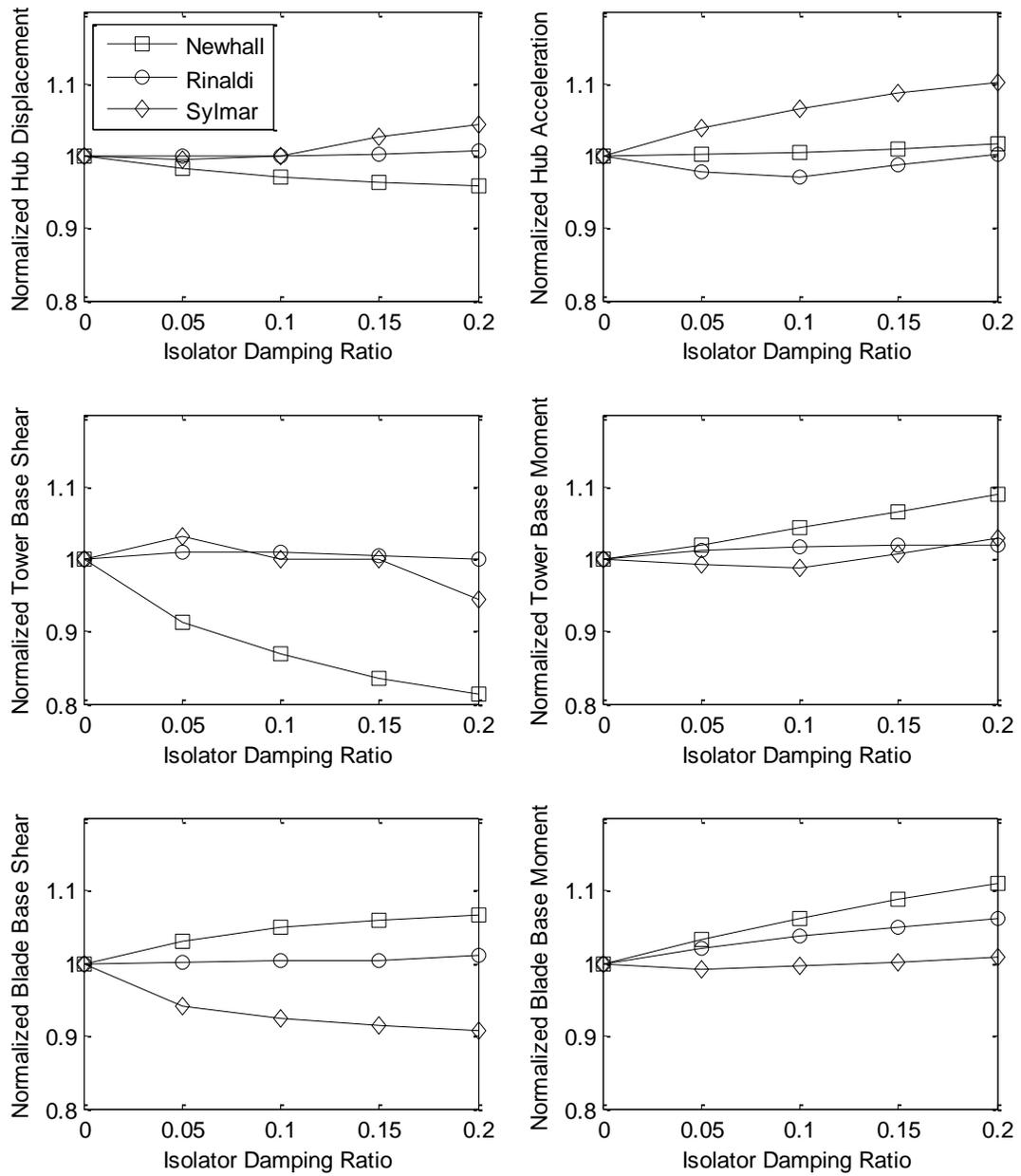
Figure 22. Peak values of key response variables under seismic loading with varied isolator damping.

The effect of increasing the isolator damping depends on the parameter in question as well as the seismic event under consideration. Most notably, increasing the degree of isolator damping tends to increase the hub acceleration and the structural response of the blades and tower in some cases. The effect of damping is complicated by the non-linear nature of the isolator, but increases in those parameters can be explained by considering the nature of the bilinear stiffness and damping components of the isolator. Bilinear stiffness allows the isolator to move freely with a low stiffness after it has yielded, which leads to decreases in many of the key response parameters. By contrast, the damping of the isolator tends to restrict the top and bottom of the isolator from translating relative to each other, and somewhat counteracts the effect of yielding. The preceding plot demonstrates that for this application of vibration isolation, the damping associated with the isolator may act to increase some structural response quantities and decrease others. The effects of isolator damping must be carefully studied to accurately predict how it will affect the turbine response under general stochastic loading.

The standard deviations of the key response variables under seismic loading with varied isolator damping are shown in Figure 23.
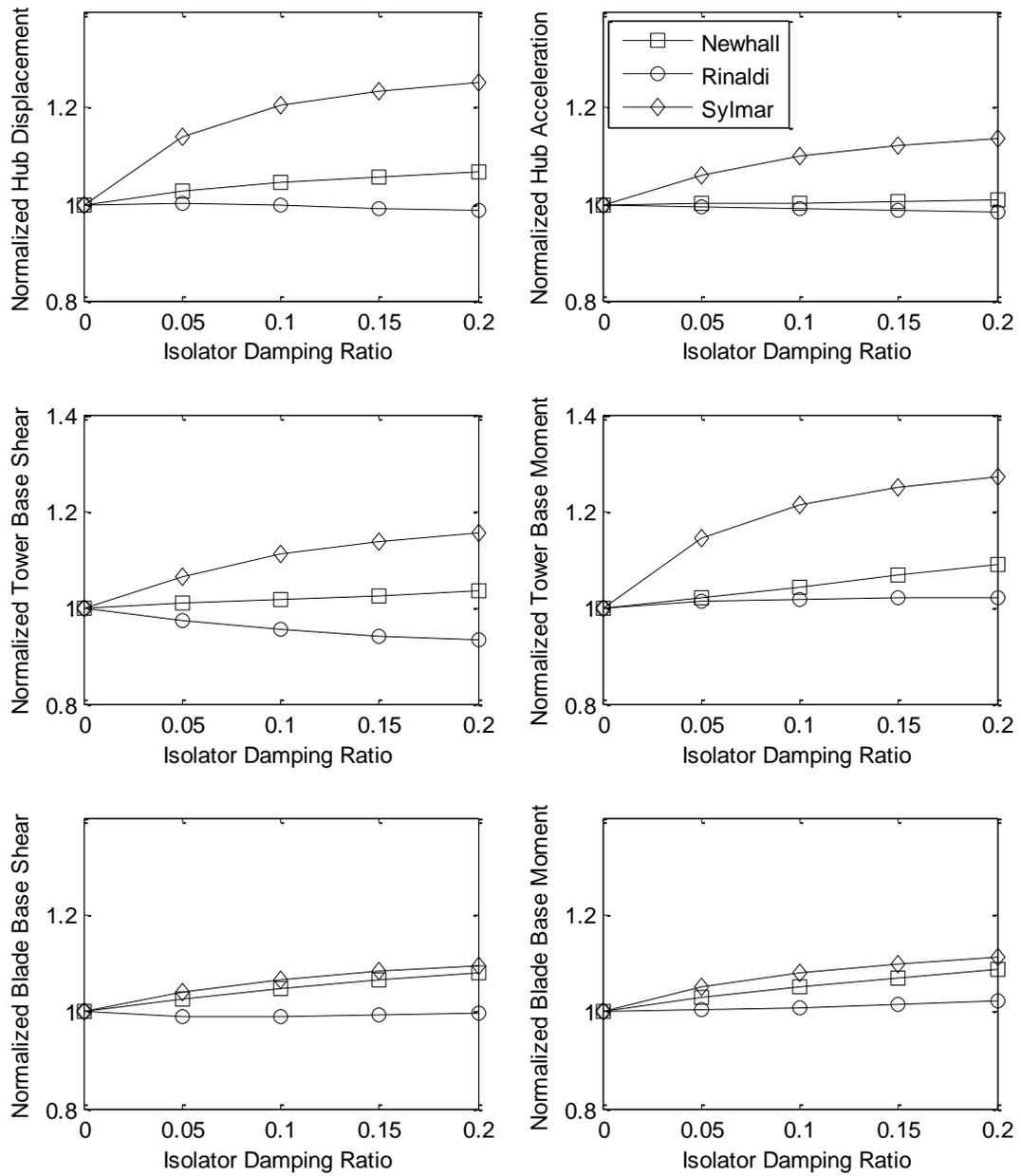
Figure 23. Standard deviation values of key response variables under seismic loading with varied isolator damping.

68

Similar to the peak values of the key parameters, the standard deviations of the key parameters are increased by isolator damping in some cases and decreased by isolator damping in others.

In addition to the key structural parameters, the effects of varied damping on the peak normalized isolator parameters are of interest. The peak values of the isolator key response variables are shown in Figure 24.
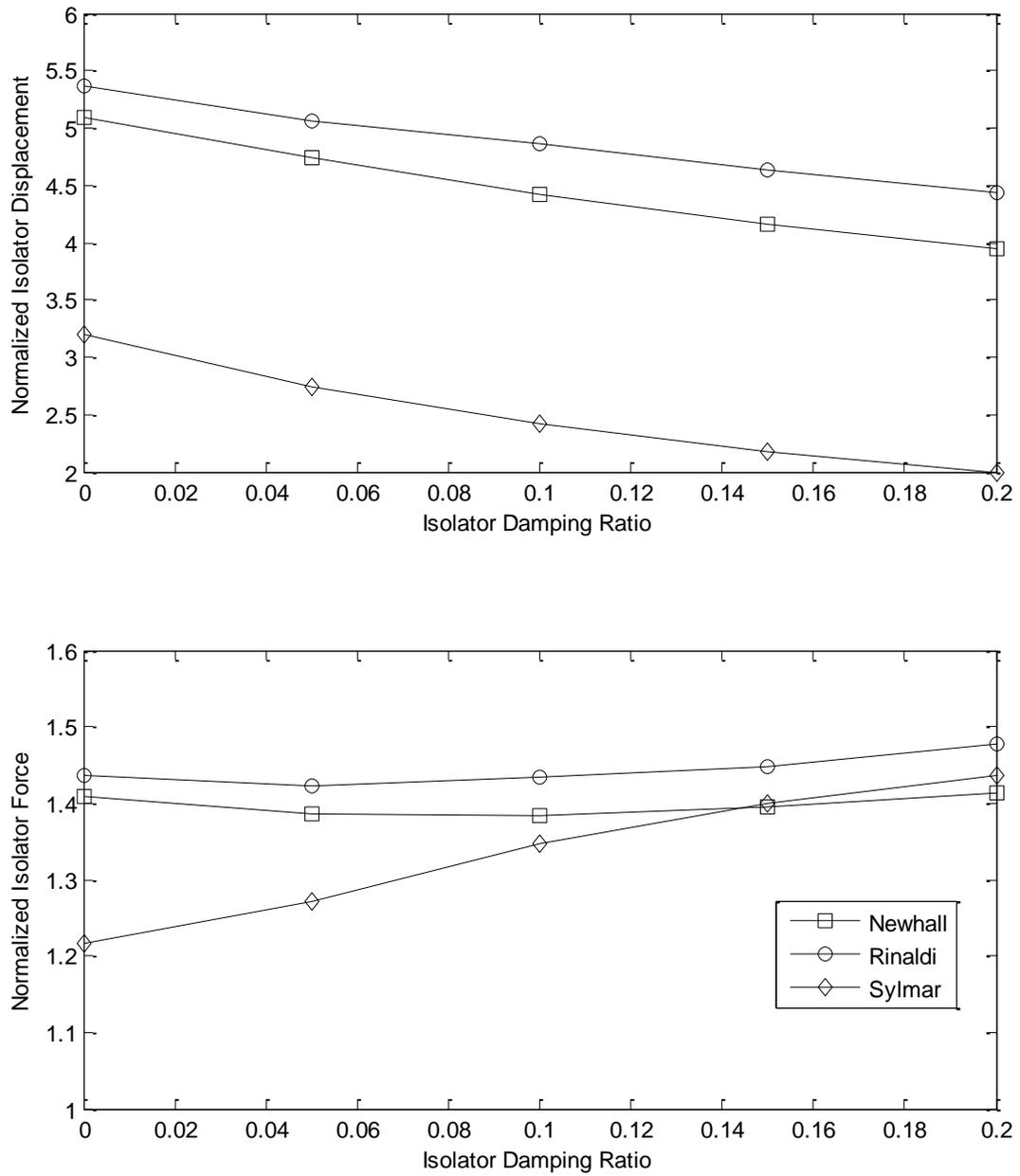
Figure 24. Peak values of isolator key response variables under seismic loading with varied isolator damping.

Increasing the degree of isolator damping causes a monotonic decrease in the normalized isolator displacement, as the damping force serves to restrict relative displacement across the isolator. The total isolator force, however, does not decrease monotonically. For the Newhall and Rinaldi events, the normalized isolator force stays relatively constant, while for the Sylmar event it increases with increasing isolator damping ratio. Again, the dependence of the normalized parameters on the damping ratio as well as the loading scenario underscore the need for robust study of the isolation system under stochastic loading.

5.2 Structural Response under Wind Loading

The un-isolated and isolated turbine structures are each subjected to a set of coherent wind speed time histories. The isolated turbine structure has an isolator yield displacement of 50 mm. Simulations are performed using initial isolator stiffness values varying from 1500 to 15000 kN/m, with an assumed damping ratio of 5% based on the initial isolator stiffness. The peak and standard deviation values of the key response variables are shown in Figure 25.
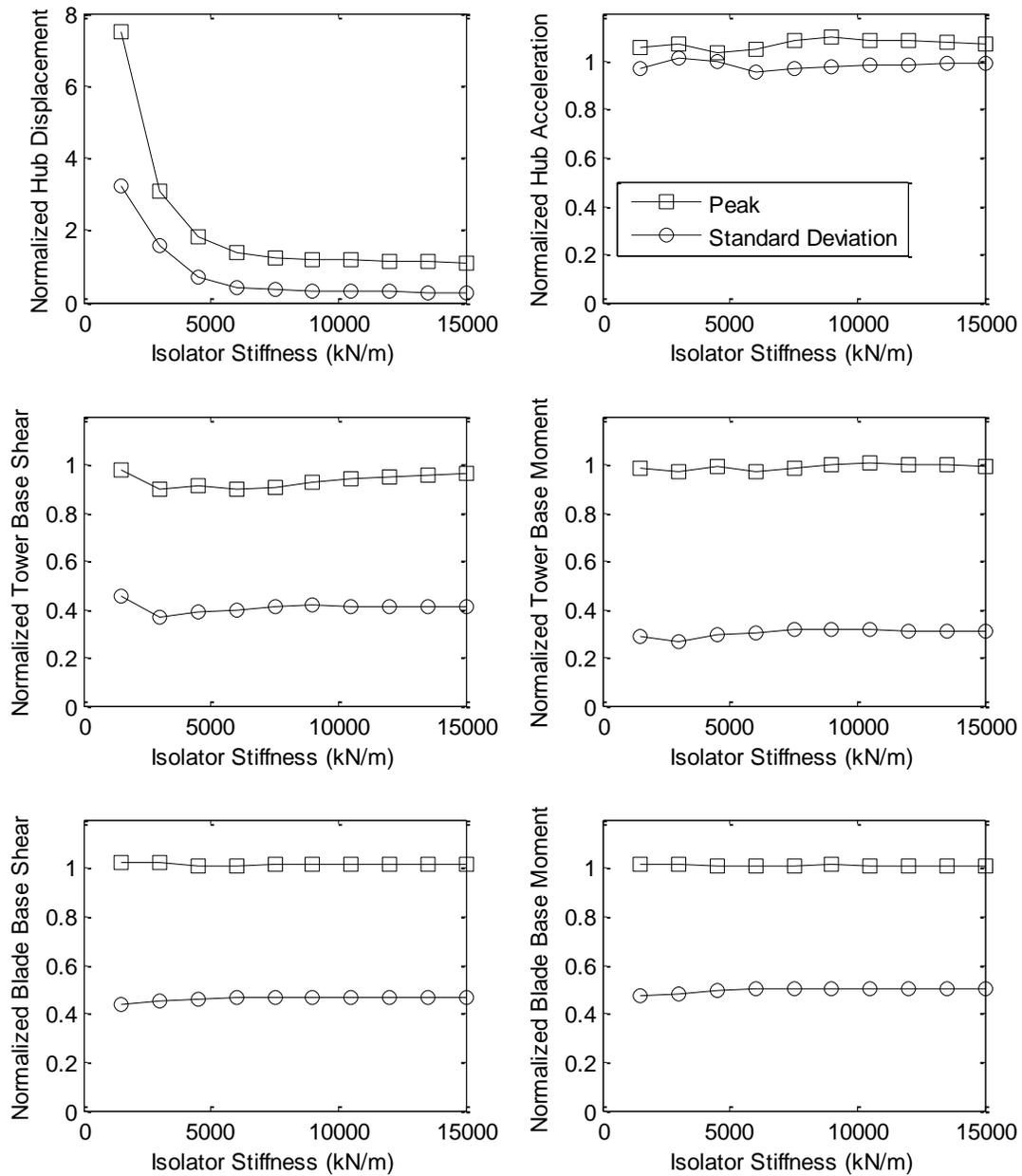
*Figure 25. Peak and standard deviation values of key response variables under wind loading with varied isolator stiffness.*

The peak hub displacement of the turbine is greatly increased for low values of isolator stiffness, while the other parameters are generally not changed significantly. The changes in response are not strongly dependent on the isolator stiffness. This result demonstrates that implementing a vibration isolator to mitigate the effect of seismic loading may not significantly change the peak structural response under wind loading, and that for the range of isolator stiffnesses considered here, the change in the structural response under wind loading is relatively constant.

The trends in the standard deviation of the key response variables are similar to the peak values. The standard deviation of the hub displacement is high for low values of isolator stiffness. The standard deviations of the other key parameters are not strongly dependent on the isolator stiffness. The variation of the structural actions on the tower and blades are greatly reduced by vibration isolator with structural parameters in the range studied here, by greater than 50% in all cases. Thus, for turbines in which isolation is implemented to mitigate response to seismic events, fatigue life may also be improved.

There is no obvious optimal value of stiffness for the structure subjected to wind loading. This is partially due to the effect of the static component of the wind force. The static components of the responses are significant, and due to the non-linear nature of the vibration isolator it is not possible to simply remove the static component from the numeric simulations. For a turbine having structural responses with greater fluctuating components, it may be possible to identify a meaningful optimal stiffness value. The peak and standard deviation values of the key response variables shown in the preceding figures are given in tabular form in Appendix B.

The objective functions for the peak and standard deviation values of the key response variables are shown in Figure 26.

73
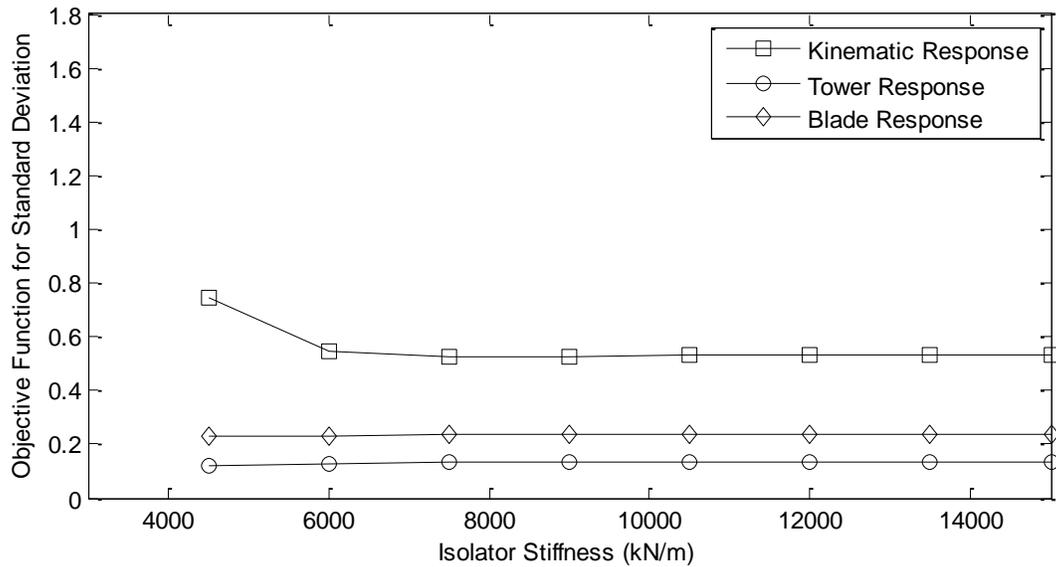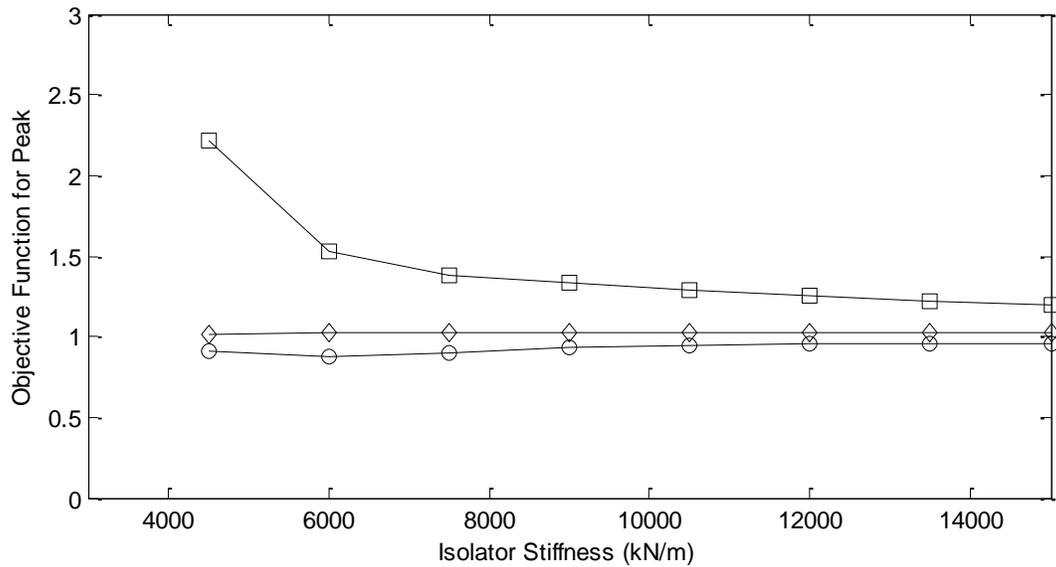
Figure 26. Objective functions for peak and standard deviation values of key response variables under wind loading with varied isolator stiffness.

As previously noted, there is not an obvious optimal stiffness value for the turbine with respect to wind loading. The objective functions are shown only for isolator stiffnesses of 4500 kN/m and above, as the objective function for kinematic response becomes extremely large at lower stiffness values. The lower stiffness values, which allow excessive isolator displacement, cannot be feasibly implemented. For the stiffness range between 5000 kN/m and 10000 kN/m which was identified as optimal for the response to seismic loading, the objective function plots show that there is little change in the peak response to wind loading and significant decreases in the standard deviation of the tower and blade response. These effects are not sensitive to changes in the isolator stiffness.

It is desirable for the isolator to yield only in extreme loading events such as earthquakes. Under the operational-level wind load considered here, yielding of the isolator may necessitate frequent re-centring, and an isolator stiffness low enough to allow yielding under operational wind loading would undergo excessive displacements under extreme wind and seismic events. These excessive displacements could pose a problem when designing the isolator for strength and stability. The normalized isolator displacement and isolator force quantities, for the 5000 kN/m to 10000 kN/m range previously identified as optimal for seismic loading, are shown in Figure 27.
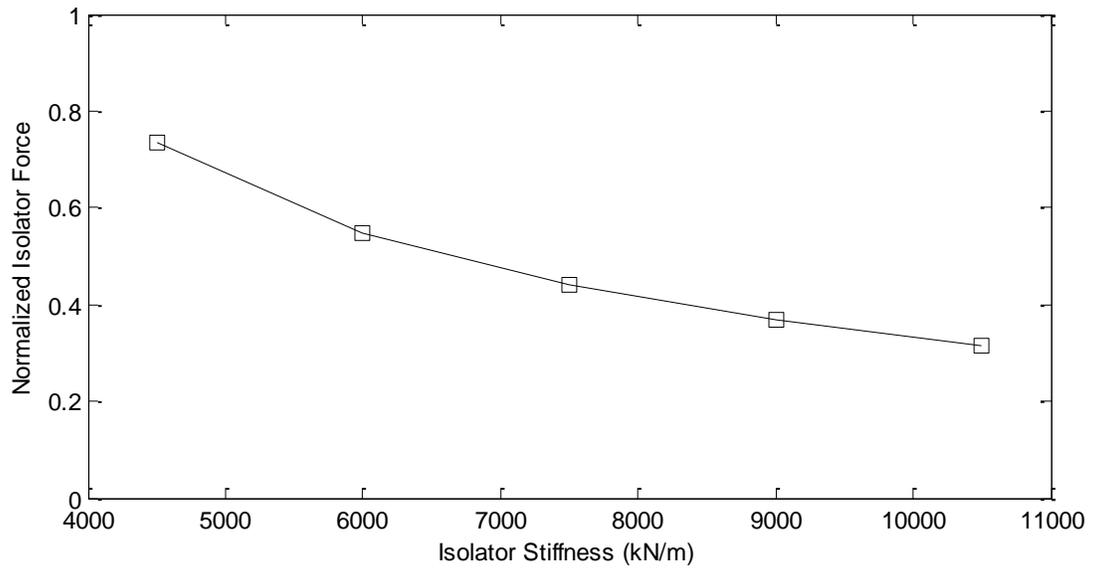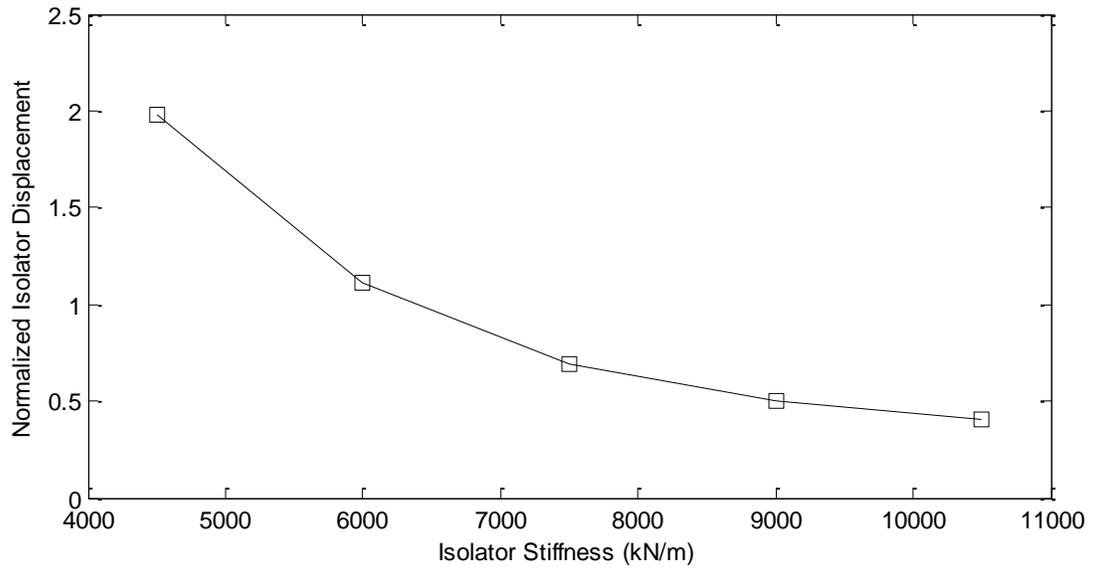
Figure 27. Peak values of isolator key response variables under wind loading with varied isolator stiffness in seismic optimal range.

76

For stiffnesses above 6000 kN/m, the peak normalized isolator displacement is less than 1, indicating that the isolator does not reach yield displacement. The isolator would remain in its elastic range for the wind loading considered, but would yield and dissipate energy in the seismic events previously considered. These stiffness values are considered to be admissible. For operational wind loading, in general, higher isolator stiffness is desirable. The peak normalized isolator displacement also decreases with increasing stiffness. It is noted that the isolator is able to reach its yield displacement without reaching its equivalent yield force, due to the repeated loading and unloading associated with turbulent wind.

The preceding investigation included simulated operational-level wind loading. For structural design of a turbine, more detailed wind loading would be considered, including deterministic gusts and direction changes, and extreme turbulence and wind speeds. It may be difficult to design a passive isolation system as described which yields in seismic events but remains in the linear elastic range for all wind loading events. In that case, a system could be designed where the isolator would yield in certain extreme wind events as well. Alternatively, a more sophisticated system could be implemented which includes some component that works as a structural fuse. The isolator would be constrained to act as a linear elastic or rigid element unless the fuse was activated by some condition, for example excessive velocity or acceleration. When the fuse was activated, the stiffness of the isolator would be decreased and the isolator would be allowed to yield or otherwise dissipate energy.

Based on the results of the preceding investigations, significant reductions in structural response can be realized by implementing vibration isolation in a wind turbine. Further research and consideration would be beneficial to develop vibration isolation as a practical option for wind turbine designers.

77

6. Conclusions

The values of the key response variables indicate that vibration isolation is a viable method to reduce the structural response of a wind turbine under seismic loading. Detailed design and implementation of vibration isolation as discussed could allow wind turbines to be deployed in seismically active areas without the need for costly strengthening and redesign to resist seismic loading. The isolation system could also decrease the standard deviation of the response to wind loading, allowing for more efficient use of material and/or increased fatigue life.

For the example turbine with an assumed yield displacement and isolator damping under seismic loading, the optimal stiffness is in the range of 5000 kN/m to 10000 kN/m. In this range, nearly all of the key response parameters are decreased relative to the un-isolated turbine. Structural response of the blades and tower are decreased in many cases by 20% or more. Under operational wind loading, the peak response of the turbine is not changed significantly, but the standard deviation of the response parameters other than hub displacement are decreased by more than 50%.

Increasing the degree of damping associated with the isolator does not have a monotonically decreasing effect on the structural response of the turbine as would be expected in an un-isolated structure. Modifying damping increases some key response parameters and decreases others, depending on the damping level and the loading scenario considered.

The results of this study demonstrate that detailed consideration of vibration isolation systems for wind turbines may lead to significant increases in structural capacity, reliability and economy. The added versatility of isolated wind turbines could contribute to the continued growth of the wind energy industry in Canada and the world.

7. Recommendations for Future Research

The main conclusion of this study is that the use of vibration isolation is an effective method of mitigating key values of wind turbine structural response. There are many aspects of this problem that are worthy of future research.

With regard to the wind turbine structure itself, a more detailed structural model would allow for the study of soil-structure interaction as well as more advanced aerodynamic behaviour of the blade cross-sections.

Methods to determine optimal parameters without performing detailed time-history analysis for the type of vibration isolator presented here, or another isolator configuration, would be beneficial to engineers seeking to implement this solution. Practical design of an isolator to achieve reduction of structural response would illuminate possible issues with implementation of such a system, and would allow for more realistic evaluation of the structural response as well as possible problems such as excessive hub displacement. Concerns such as failsafe systems should be considered.

Testing is generally required to verify the physical properties of vibration isolators; in order to better understand the dynamics, scale models could be designed and tested on a bench-scale using a load actuator, or on a larger scale using a shake table.

Finally, practical design of structures with vibration isolators, energy-dissipating elements and the like is greatly complicated in its early stages by the lack of a simple, codified design method. Ultimately, it would be desirable to develop such a design method, based on the results of detailed parametric study and statistical analysis, in order to encourage more widespread use of isolation technology among practicing engineers.

References

Burton, T., Sharpe, D., Jenkins, N., & Bossanyi, E. (2001). Wind Energy Handbook. West Sussex, England: John Wiley & Sons, Ltd.

Colwell, S. & Basu, B. (2009). Tuned liquid column dampers in offshore wind turbines for structural control. *Engineering Structures*, 31:358-368.

COMSOL Support (2011). BDF vs. Generalized Alpha time discretization, *COMSOL Support Knowledge Base*, <www.comsol.com/support/knowledgebase/>.

Craig, R.R., & Kurdila, A.J. (2006). Fundamentals of Structural Dynamics. Hoboken, NJ: John Wiley & Sons, Inc.

Dueñas-Osorio, L., & Basu, B. (2008). Unavailability of wind turbines due to wind-induced accelerations. *Engineering Structures*, 30: 885-893.

Hall, J.F. (2006). Problems encountered from the use (or misuse) of Rayleigh damping. *Earthquake Engineering and Structural Dynamics*, 35: 525-545.

Hansen, M. (2008). Aerodynamics of Wind Turbines. London, England: Earthscan.

Hurty, W.C. (1965). Vibration of structural systems by component mode synthesis. *Journal of the Engineering Mechanics Division, Proceedings of the American Society of Civil Engineers*, 4: 51-69

IEC 61400-1:2007: Wind Turbines – Part 1: Design requirements (2007). International Electrotechnical Commission, Geneva, Switzerland.

Ismail, M., Ikhouane, F., & Rodellar, J. (2009). The Hysteresis Bouc-Wen Model, A Survey. *Archives of Computational Methods in Engineering*, 16: 161-188.

Marano, G.C. & Sgobba, S. (2007). Stochastic energy analysis of seismic isolated bridges. *Soil Dynamics and Earthquake Engineering*, 27: 759-773.

Murtagh, P.J., Basu, B., & Broderick, B.M. (2004). Simple models for natural frequencies and mode shapes of towers supporting utilities. *Computers & Structures*, 82: 1745-1750.

Murtagh, P.J., Basu, B., & Broderick, B.M. (2005). Along-wind response of a wind turbine tower with blade coupling subjected to rotationally sampled wind loading. *Engineering Mechanics*, 27: 1209-1219.

Murtagh, P.J., Ghosh, A., Basu, B., & Broderick, B.M. (2008). Passive control of wind turbine vibrations including blade/tower interaction and rotationally sampled wind loading. *Wind Energy*, 11: 305-317.

Naguleswaran, S. (1994). Lateral vibration of a centrifugally tensioned uniform Euler-Bernoulli beam. *Journal of Sound and Vibration*, 176(5): 613-624.

Narasimhan, S., Nagarajaiah, N., Johnson, E.A., & Gavin, H.P. (2006). Smart base-isolated benchmark building. Part I: problem definition. *Structural Control and Health Monitoring*, 13: 573-588.

Naiem, F. & Kelly, J.M. (1999). Design of Seismic Isolated Structures: From Theory to Practice. New York, NY: John Wiley & Sons, Inc.

Prowell, I., Veletsos, M., & Elgamal, A. (2008). Full Scale Testing For Investigation of Wind Turbine Seismic Response. *Proceedings of the 7th World Wind Energy Conference*, Kingston, Ontario, Canada.

Prowell, I. & Veers, P.S. (2008). Assessment of Wind Turbine Seismic Risk: Existing Literature and Simple Study of Tower Moment Demand. *Sandia Report SAND2009-1100*, Sandia National Laboratories, Albuquerque, NM.

Simiu, E., & Scanlan, R. (1996). Wind Effects on Structures. New York, NY: Wiley-Interscience.

Timmer, W.A. (2010). Aerodynamic characteristics of wind turbine blade airfoils at high angles-of-attack. *Proceedings of Torque 2010: The Science of Making Torque from Wind*, Crete, Greece.

Veers, P.S. (1988). Three-Dimensional Wind Simulation. *Sandia Report SAND88-0152*, Sandia National Laboratories, Albuquerque, NM.

Weaver, W., & Gere, J.M. (1980). Matrix Analysis of Framed Structures. New York, NY: D. Van Nostrand Company.

Wen, Y.K. (1976). Method for random vibration of hysteretic systems. *Journal of Engineering Mechanics*, 102: 249-263.

Witcher, D. (2005). Seismic analysis of wind turbines in the time domain. *Wind Energy*, 8:81-91.

Ziyaeifar, M. & Noguchi, H. (1998). Partial mass isolation in tall buildings. *Earthquake Engineering and Structural Dynamics*, 27: 49-65.

Appendix A – Vibration Modes of Un-Isolated Structure

Description of Natural Mode	Image
Along-wind tower bending mode Natural frequency = 0.567 Hz Modal participating mass ratio in along-wind direction = 63.2%	
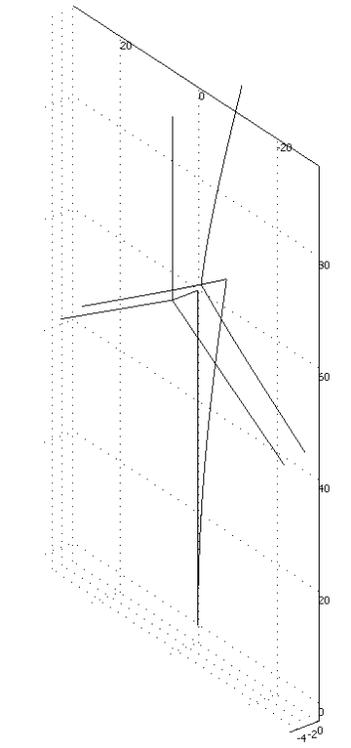
Along-wind blade bending mode

Natural frequency = 1.413 Hz

Modal participating mass ratio in along-wind
direction = 1.9%
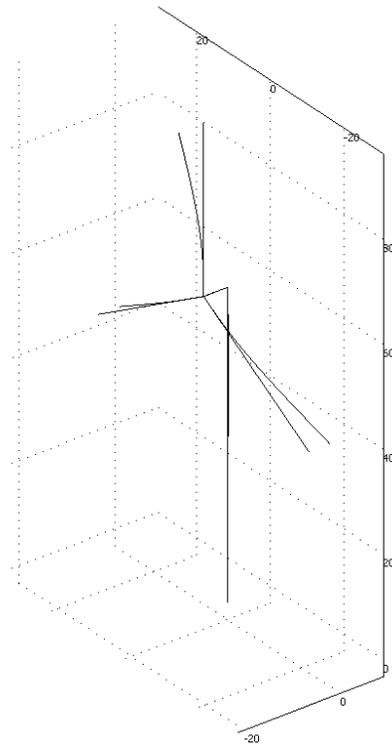
Along-wind blade bending mode

Natural frequency = 1.536Hz

Modal participating mass ratio in along-wind
direction = 1.4%
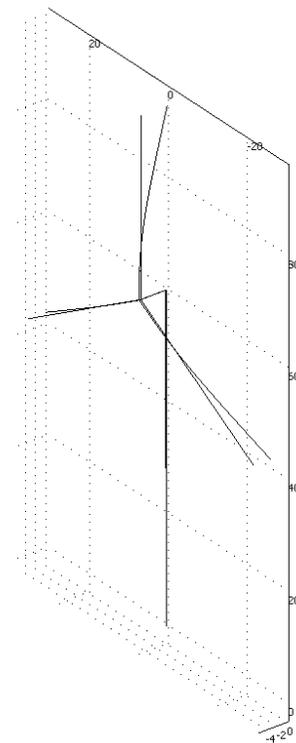
Along-wind blade and tower bending mode

Natural frequency = 3.606 Hz

Modal participating mass ratio in along-wind direction = 2.6%
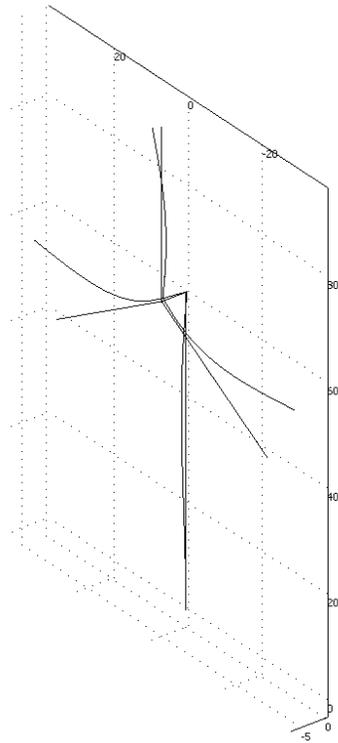
Along-wind tower and blade bending mode

Natural frequency = 4.201 Hz

Modal participating mass ratio in along-wind direction = 12.7%
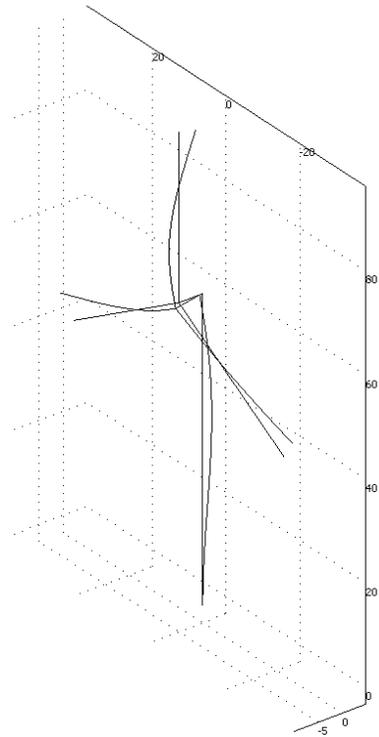
Appendix B – Tables of Structural Key Response Variables and Relative Changes

Table B1 – Response to Newhall Seismic Loading

| Parameter of Interest		No Isolator Base Value	Values Normalized to No Isolator Base Value									
			Isolator Stiffness (kN/m)									
			1500	3000	4500	6000	7500	9000	10500	12000	13500	15000
Hub Displacement (m)	Peak	0.536	0.972	0.876	0.785	0.915	1.000	1.002	0.998	1.008	1.022	1.028
	SD	0.218	0.685	0.549	0.674	0.816	0.946	1.073	1.159	1.197	1.223	1.229
Hub Acceleration (g)	Peak	1.352	0.551	0.622	0.685	0.780	0.837	0.862	0.854	0.955	1.044	1.107
	SD	0.345	0.493	0.589	0.708	0.812	0.886	0.956	1.019	1.062	1.096	1.116
Tower Base Shear (kN)	Peak	1501.6	0.823	0.794	0.687	0.595	0.608	0.526	0.562	0.621	0.730	0.814
	SD	417.4	0.561	0.514	0.557	0.654	0.753	0.863	0.954	1.011	1.055	1.082
Tower Base Moment (kN*m)	Peak	51962.6	0.678	0.589	0.548	0.639	0.684	0.715	0.794	0.924	0.999	1.029
	SD	20490.9	0.346	0.351	0.475	0.629	0.769	0.913	1.014	1.069	1.110	1.129
Blade Base Shear (kN)	Peak	155.2	1.285	1.017	0.822	0.769	0.781	0.814	0.874	0.959	0.921	0.969
	SD	45.9	1.052	0.920	0.767	0.703	0.722	0.797	0.878	0.920	0.951	0.967
Blade Base Moment (kN*m)	Peak	3261.2	1.258	0.972	0.763	0.670	0.684	0.749	0.795	0.835	0.846	0.853
	SD	908.9	1.135	0.986	0.808	0.722	0.722	0.784	0.861	0.901	0.928	0.944

Table B2 – Response to Rinaldi Seismic Loading

Parameter of Interest		No Isolator Base Value	Values Normalized to No Isolator Base Value									
			Isolator Stiffness (kN/m)									
			1500	3000	4500	6000	7500	9000	10500	12000	13500	15000
Hub Displacement (m)	Peak	0.678	0.942	0.844	0.778	0.803	0.855	0.892	0.926	0.953	0.964	0.968
	SD	0.265	0.628	0.592	0.612	0.634	0.631	0.604	0.601	0.632	0.681	0.735
Hub Acceleration (g)	Peak	1.692	0.629	0.707	0.764	0.808	0.809	0.824	0.856	0.887	0.924	0.964
	SD	0.434	0.430	0.492	0.561	0.639	0.672	0.682	0.715	0.731	0.767	0.796
Tower Base Shear (kN)	Peak	1326.5	1.247	1.097	0.983	0.892	0.836	0.812	0.797	0.784	0.836	0.862
	SD	481.4	0.583	0.495	0.493	0.548	0.566	0.558	0.587	0.604	0.649	0.687
Tower Base Moment (kN*m)	Peak	62923.1	0.727	0.551	0.587	0.611	0.588	0.640	0.700	0.700	0.787	0.858
	SD	24503.1	0.370	0.334	0.396	0.475	0.507	0.509	0.527	0.562	0.615	0.671
Blade Base Shear (kN)	Peak	195.8	0.991	0.739	0.789	0.807	0.792	0.863	0.927	0.951	0.963	0.988
	SD	41.9	1.022	0.861	0.807	0.738	0.685	0.686	0.716	0.738	0.763	0.793
Blade Base Moment (kN*m)	Peak	3620.4	1.081	0.821	0.778	0.763	0.774	0.824	0.879	0.905	0.919	0.934
	SD	760.4	1.157	0.972	0.899	0.807	0.730	0.729	0.763	0.783	0.804	0.830

Table B3 – Response to Sylmar Seismic Loading

Parameter of Interest		No Isolator Base Value	Values Normalized to No Isolator Base Value									
			Isolator Stiffness (kN/m)									
			1500	3000	4500	6000	7500	9000	10500	12000	13500	15000
Hub Displacement (m)	Peak	0.618	0.849	0.730	0.670	0.638	0.622	0.636	0.702	0.761	0.797	0.828
	SD	0.319	0.476	0.358	0.347	0.393	0.486	0.563	0.655	0.736	0.786	0.825
Hub Acceleration (g)	Peak	1.796	0.547	0.594	0.626	0.652	0.673	0.692	0.715	0.739	0.761	0.805
	SD	0.462	0.312	0.348	0.396	0.444	0.509	0.578	0.651	0.712	0.756	0.797
Tower Base Shear (kN)	Peak	1615.0	0.462	0.531	0.548	0.524	0.628	0.746	0.736	0.653	0.680	0.698
	SD	582.5	0.302	0.298	0.315	0.356	0.426	0.496	0.574	0.642	0.693	0.739
Tower Base Moment (kN*m)	Peak	66151.5	0.338	0.382	0.425	0.472	0.553	0.609	0.614	0.604	0.638	0.679
	SD	29728.6	0.194	0.212	0.257	0.321	0.411	0.488	0.579	0.660	0.714	0.759
Blade Base Shear (kN)	Peak	113.8	1.112	0.886	0.808	0.904	0.945	0.885	1.001	1.064	0.943	0.918
	SD	42.4	0.665	0.519	0.460	0.502	0.555	0.615	0.676	0.728	0.764	0.796
Blade Base Moment (kN*m)	Peak	1882.3	1.303	1.021	0.865	0.920	0.960	0.969	0.991	0.981	0.933	0.951
	SD	720.9	0.797	0.608	0.518	0.552	0.599	0.658	0.710	0.756	0.790	0.821

Table B4 – Response to Wind Loading

Parameter of Interest		No Isolator Base Value	Values Normalized to No Isolator Base Value									
			Isolator Stiffness (kN/m)									
			1500	3000	4500	6000	7500	9000	10500	12000	13500	15000
Hub Displacement (m)	Peak	0.111	7.497	3.074	1.831	1.394	1.259	1.208	1.176	1.151	1.128	1.108
	SD	0.034	3.230	1.581	0.705	0.421	0.341	0.314	0.302	0.296	0.290	0.286
Hub Acceleration (g)	Peak	0.063	1.061	1.075	1.037	1.052	1.089	1.100	1.089	1.089	1.082	1.076
	SD	0.020	0.973	1.012	0.997	0.960	0.967	0.978	0.984	0.989	0.990	0.990
Tower Base Shear (kN)	Peak	205.0	0.991	0.904	0.915	0.898	0.912	0.928	0.946	0.958	0.966	0.974
	SD	56.1	0.422	0.301	0.311	0.312	0.325	0.336	0.343	0.348	0.351	0.354
Tower Base Moment (kN*m)	Peak	10288.7	0.992	0.973	0.989	0.970	0.980	0.997	1.002	1.004	1.000	0.997
	SD	868.2	0.277	0.234	0.251	0.240	0.253	0.265	0.272	0.277	0.279	0.280
Blade Base Shear (kN)	Peak	68.6	1.026	1.020	1.010	1.012	1.015	1.015	1.015	1.014	1.014	1.012
	SD	17.6	0.440	0.449	0.462	0.465	0.465	0.466	0.466	0.466	0.466	0.466
Blade Base Moment (kN*m)	Peak	1378.0	1.019	1.016	1.009	1.011	1.012	1.012	1.012	1.011	1.010	1.010
	SD	346.2	0.476	0.484	0.497	0.500	0.501	0.501	0.502	0.502	0.502	0.502

Appendix C – MATLAB Code for Wind Speed Generation

```matlab
% Script "Wind" created by Chad Van der Woude, University of Waterloo
%
% This script simulates a set of wind speed time histories having a given
% power spectral density and coherence, as prescribed by IEC 61400-1.
% The methodology used is based on the reference (Hansen, 2008) in the text
% of the author's MASc thesis document.


flow = 1/40; % Low frequency (Hz)
fhigh = 10; % High frequency (Hz)


rad = 12; % Number of radial lines to simulate for wind
num = 10; % Number of points along each radial line
fL = 33; % Length of blade including hub radius
hL = 3; % Hub radius of blade
HH = 60; % Hub height
numT = 10; % Number of points to simulate along the tower height
NH = 2; % Nacelle height


Tr = 10; % Ramp time for wind speed up to maximum.
alpha = 0.2; % Power law coefficient


Trev = 3.5; % Revolution period


L = fL-hL; % Length of blade without hub radius
dL = L/num; % Length of each blade section
ang = 2*pi/rad; % Angle between radial lines


T = 1/flow; % Calculate time to be simulated (s)
N = fhigh*2*T; % Calculate number of time instants to simulate
nF = T*fhigh; % Number of frequencies
dt = T/N; % Time differential
dF = 1/T; % Frequency differential


% Populate time vector
time = zeros(N,1);
for c1 = 1:N
    time(c1,1) = c1*dt;
end


% Properties of wind
V = 10; % Wind speed (m/s)
I = 0.18; % Turbulence intensity
sd = I*V; % Calculate standard deviation (m/s)
Ls = 340; % Length scale (m)


npts = rad*num+numT;
pts = zeros(npts,2);
% This set of loops defines the coordinates at which time-histories are
% simulated so that their separation distances can be found to calculate
% coherence.
display('Defining point coordinates.')
for c1 = 1:num;
    for c2 = 1:rad;
        numpt = c2+(c1-1)*rad;
        az = (c2-1)*ang;
```

93

```
        pts(numpt,1) = (hL + (c1-0.5)*dL)*cos(pi/2-az);
        pts(numpt,2) = HH+(hL + (c1-0.5)*dL)*sin(pi/2-az);
    end
end
for c1 = 1:numT
    numpt = rad*num+c1;
    pts(numpt,1) = 0;
    pts(numpt,2) = ((HH-NH)/numT)*(c1-0.5);
end

display('Populating spectral matrix.')
% This set of loops populates the spectral matrix S
S = zeros(npts,npts,nF);
Ssum = zeros(npts,npts);
for c1 = 1:npts
    for c2 = 1:npts
        for c3 = 1:nF
            sep = ((pts(c1,1)-pts(c2,1))^2+(pts(c1,2)-pts(c2,2))^2)^0.5;
            freq = c3/T;
            S(c1,c2,c3) = exp(-
12*((freq*sep/V)^2+(0.12*sep/Ls)^2)^0.5)*(4*sd^2*Ls/V)/(1+6*freq*Ls/V)^(5/3);
        end
    end
end

display('Populating H matrix.')
% This set of loops populates the matrix H by a recursive scheme.
H = zeros(npts,npts,nF);
for c1 = 1:nF
    H(1,1,c1) = sqrt(S(1,1,c1));
    H(2,1,c1) = S(2,1,c1)/H(1,1,c1);
    H(2,2,c1) = (S(2,2,c1)-H(2,1,c1)^2)^0.5;
    for c2 = 3:npts
        for c3 = 1:c2
            if c3 ~= 1
                sum1 = 0;
                sum2 = 0;
                for c4 = 1:(c3-1)
                    sum1 = sum1 + H(c3,c4,c1)^2;
                    sum2 = sum2 + H(c2,c4,c1)*H(c3,c4,c1);
                end
            end
            if c3 == 1
                H(c2,c3,c1) = S(c2,c3,c1)/H(c3,c3,c1);
            elseif c2 == c3
                H(c2,c3,c1) = (S(c2,c3,c1) - sum1)^0.5;
            else
                H(c2,c3,c1) = (S(c2,c3,c1)-sum2)/H(c3,c3,c1);
            end
        end
    end
end

display('Determining phase angles.')
% Determine random phase angles
phi = zeros(npts,nF);
```

94

```matlab
for c1 = 1:npts
    for c2 = 1:nF
        phi(c1,c2) = rand*2*pi;
    end
end

display('Populating vectors for wind field generation.')
% Populate "Real", "Imag", "Amp", "Pha" vectors
Real = zeros(npts,nF);
Imag = zeros(npts,nF);
Amp = zeros(npts,nF);
Pha = zeros(npts,nF);
for c1 = 1:npts
    for c2 = 1:nF
        for c3 = 1:c1
            Real(c1,c2) = Real(c1,c2) + H(c1,c3,c2)*cos(phi(c3,c2));
            Imag(c1,c2) = Imag(c1,c2) + H(c1,c3,c2)*sin(phi(c3,c2));
            Amp(c1,c2) = sqrt(Real(c1,c2)^2 + Imag(c1,c2)^2);
            if Imag(c1,c2) > 0
                if Real(c1,c2) > 0
                    Pha(c1,c2) = atan(Imag(c1,c2)/Real(c1,c2));
                else
                    Pha(c1,c2) = pi - atan(abs(Imag(c1,c2)/Real(c1,c2)));
                end
            else
                if Real(c1,c2) > 0
                    Pha(c1,c2) = 2*pi - atan(abs(Imag(c1,c2)/Real(c1,c2)));
                else
                    Pha(c1,c2) = pi + atan(abs(Imag(c1,c2)/Real(c1,c2)));
                end
            end
        end
    end
end

display('Generating time histories.')
% Generate fluctuating time histories
u = zeros(npts,N);
for c1 = 1:npts
    for c2 = 1:N
        for c3 = 1:nF
            u(c1,c2) = u(c1,c2) + 2*Amp(c1,c3)*cos(2*pi*(c3/T)*(c2*dt)-
Pha(c1,c3));
        end
    end
end

display('Normalizing time histories.')
% Normalize fluctuating time histories and generate total time history.
for c1 = 1:npts
    sdbefore = std(u(c1,:));
    u(c1,:) = (sd/sdbefore)*u(c1,:);
    for c2 = 1:N
        u(c1,c2) = u(c1,c2) + V;
    end
end
```

```
% This section of the code organizes the generated time-histories into a
% format that can be exported to COMSOL for application to the structural
% model.

display('STATIONARY WIND TIME HISTORIES')
uSb = zeros(3*num*N,3);
uSt = zeros(numT*N,3);

display('Creating time histories for output.')
display('Creating time history for blade 1.')
for c1 = 1:rad:rad*num-2/3*rad
    newC = floor(c1/rad)*3+1;
    uSb(1+(newC-1)*N:newC*N,1) = ones(N,1)*newC;
    uSb(1+(newC-1)*N:newC*N,2) = time;
    uSb(1+(newC-1)*N:newC*N,3) = u(c1,:);
end
display('Creating time history for blade 2.')
for c1 = 1+rad/3:rad:rad*num-1/3*rad
    newC = floor(c1/rad)*3+2;
    uSb(1+(newC-1)*N:newC*N,1) = ones(N,1)*newC;
    uSb(1+(newC-1)*N:newC*N,2) = time;
    uSb(1+(newC-1)*N:newC*N,3) = u(c1,:);
end
display('Creating time history for blade 3.')
for c1 = 1+2*rad/3:rad:rad*num
    newC = floor((c1-1)/rad)*3+3;
    uSb(1+(newC-1)*N:newC*N,1) = ones(N,1)*newC;
    uSb(1+(newC-1)*N:newC*N,2) = time;
    uSb(1+(newC-1)*N:newC*N,3) = u(c1,:);
end
display('Creating time history for tower.')
for c1 = num*rad+1:num*rad+numT
    uSt(1+(c1-num*rad-1)*N:(c1-num*rad)*N,1) = ones(N,1)*(c1-num*rad);
    uSt(1+(c1-num*rad-1)*N:(c1-num*rad)*N,2) = time;
    uSt(1+(c1-num*rad-1)*N:(c1-num*rad)*N,3) = u(c1,:);
end

% This sections samples the wind time histories to approximate the
% time-history that a rotating blade would be subjected to.

display('ROTATIONAL WIND TIME HISTORIES')
sector = zeros(rad+1,1);
for c1 = 1:rad
    sector(c1,1) = (c1-1)*Trev/rad;
    sector(c1,2) = c1;
end
sector(rad+1,1) = Trev;
sector(rad+1,2) = 1;

uRb = zeros(3*num*N,3);

display('Creating time histories for output.')
display('Creating time history for blades.')
for c1 = 1:N
```

```matlab
        [mindiff closest] = min(abs(sector(:,1) - mod(time(c1),Trev)));
        count = 0;
        for c2 = 1:rad:rad*num-2/3*rad
            newC = floor(c2/rad)*3+1;
            cr = floor(c2/rad)*rad+sector(closest,2);
            uRb(c1+(newC-1)*N,1) = newC;
            uRb(c1+(newC-1)*N,2) = time(c1);
            uRb(c1+(newC-1)*N,3) = u(cr,c1);
        end
        [mindiff closest] = min(abs(sector(:,1) - mod(time(c1)+1/3*Trev,Trev)));
        for c2 = 1+rad/3:rad:rad*num-1/3*rad
            newC = floor(c2/rad)*3+2;
            cr = floor(c2/rad)*rad+sector(closest,2);
            uRb(c1+(newC-1)*N,1) = newC;
            uRb(c1+(newC-1)*N,2) = time(c1);
            uRb(c1+(newC-1)*N,3) = u(cr,c1);
        end
        [mindiff closest] = min(abs(sector(:,1) - mod(time(c1)+2/3*Trev,Trev)));
        for c2 = 1+2*rad/3:rad:rad*num
            newC = floor(c2/rad)*3+3;
            cr = floor(c2/rad)*rad+sector(closest,2);
            uRb(c1+(newC-1)*N,1) = newC;
            uRb(c1+(newC-1)*N,2) = time(c1);
            uRb(c1+(newC-1)*N,3) = u(cr,c1);
        end
    end
end
display('Creating time history for tower.')
uRt = uSt;

display('Conditioning time histories for ramp-in.')
for c1 = 1:3*num*N
    if uSb(c1,2) <= 10
        uSb(c1,3) = uSb(c1,2)/10*uSb(c1,3);
    end
    if uRb(c1,2) <= 10
        uRb(c1,3) = uRb(c1,2)/10*uRb(c1,3);
    end
end
for c1 = 1:numT*N
    if uSt(c1,2) <= 10
        uSt(c1,3) = uSt(c1,2)/10*uSt(c1,3);
    end
    if uRt(c1,2) <= 10
        uRt(c1,3) = uRt(c1,2)/10*uRt(c1,3);
    end
end

display('Applying wind profile to tower.')
for c1 = 1:numT*N
    uSt(c1,3) = uSt(c1,3)*(pts(rad*num+uSt(c1,1),2)/HH)^alpha;
    uRt(c1,3) = uRt(c1,3)*(pts(rad*num+uRt(c1,1),2)/HH)^alpha;
end

display('Complete!')
```